Digital In-Line Holography with Extreme Ultraviolet Radiation

Master's Thesis
by
Nils Adie

Abstract

This diploma thesis is a first step towards a successful implementation of digital in-line holography with extreme ultra violet radiation. The underlying principles of both high harmonic generation and holography are described, and an explicit description of the holographic reconstruction algorithm is provided. The reconstruction algorithm is subjected to a thorough simulation before being confronted with experimental conditions. Three holographic experiments have been carried out – each more complicated than the previous. These experiments provide the stepping-stones for the further implementation of the results. The thesis concludes that for holography to be successfully carried out with harmonics several improvements need to be made. It seems to be imperative that one harmonic is isolated in order to receive a clear image. Further, the resolution of the setup needs to be drastically increased to warrant further exerts. This can be done either by magnification or by increasing the distance between the object and the recording devices and acquiring devices with better resolution.

Key words: Digital in-line holography, Harmonic generation, Reconstruction algorithm

Contents

List of Figures

Chapter 1

Introduction

1.1 Background and Motivation

The topic of this thesis can crudely be divided into two parts; harmonics and holography. The harmonics in this thesis are created by focusing pulses emanating from the terawatt laser at the Lund Laser Centre in Argon gas. One way of viewing what happens is that this seriously disrupts the potential well the Argon electrons experience. They briefly leave the atom and are accelerated in the electric field of the pulse before recombining with the host atom. The energy released during the process is the harmonic pulse which exhibits coherence properties similar to that of the laser.

Holography simply makes use of the postulate that a wave front can be viewed as plane from which an infinite amount of wavelets originate. Knowing the behaviour of each of these wavelets, the wave front at another point in space along its axes of propagation can be recreated. In conventional holography two beams are used. One is the reference beam, which is aimed directly at a recording medium. The other is the object beam, which is shone onto an object. Interference takes place at the recording medium between the reference beam and the light scattered from the object, creating a hologram. In in-line holography only one beam is used. This entails a loss of information although stability is gained. In digital holography the recording medium is a CCD camera. The recorded hologram can be used to recreate an image of the original object. This is done through digitally subjecting the hologram to a wave with the same properties as the reference wave.

The goal of this thesis has been to perform holography with high harmonics. The source of inspiration was an article by Bartels et al where digital in-line holography was performed on a tabletop setup [1]. They used a Ti:sapphire laser at 760 nm with a pulse duration of 25 fs to create harmonics of orders 17 through to 23. An aluminium filter blocked the fundamental and objects were inserted into the beam. The resulting interference patterns, or in-line holograms, were recorded by an X-ray CCD camera further down the beam path. A geometric magnification of projection of the setup combined with a resolution of the CCD camera of 26μm led to a resolution of the reconstructed images of 6.8μm in the best case.

The field of research is extremely interesting and the long-term prospects are fascinating. Using harmonics seems to make it possible to use holography for viewing much smaller objects than has been possible previously. The reason for this is that harmonics exhibit the necessary coherence properties crucial for performing holography while

being of a short wavelength. By glancing towards groups performing holography with coherent electron beams, a future where in-line holography with high harmonics can be used for imaging objects in the nanometer region in 3D does not seem impossible [8]. Further, the prospect of performing holography with femtosecond time resolution seems viable[1].

1.2   Outline

The first main chapter of the thesis addresses holography. After a brief introduction to the concept of holography in general, conventional and in-line holography are addressed in more detail. The following sections contain an explicit presentation of the reconstruction algorithm used and a simulation of the holographic reconstruction process. The next chapter deals with harmonic generation. After a brief description of the underlying principle and a presentation of the setup used, the process of optimising and spectrally filtering the harmonic beam is attended to. Chapter 4 describes the experiments carried out and discusses the results. Finally, the last chapter contains the conclusions that can be drawn from the work carried out and contains a discussion on which efforts could be made to improve various aspects of the results.

Chapter 2

Holography

In this chapter two different kinds of holography will be described after a brief introduction to holography in general. Conventional, or off-line, holography will be presented first. Conventional holography is the kind of holography that generally springs to mind when the topic is brought up. However, Gabor's original thoughts on holography were more along the lines of in-line holography, which the third section of this chapter will cover. The fourth section will address how digital in-line holography is made feasible through reconstruction algorithms. Finally the chapter will be rounded up with a presentation of the simulation that was done in order to discern between effects due to the variation of various key parameters.

2.1   A General Introduction to Holography

Dennis Gabor is usually recognised as the inventor of holography. In 1948 he realised that the process of recording an interference pattern on a photographic plate and recreating a picture of the original object with a beam with relevant properties could be useful for microscopic purposes. Gabor came up with the idea of holography as a way of improving electron microscopy so that atomic lattices could be resolved.

The basic idea behind holography is to use the interference between a coherent beam scattered off an object and a coherent reference beam. The interference pattern can then be recorded, either photographically or digitally, in order to reproduce an image of the original object [3].

2.2   Conventional Holography

A basic setup for recording a conventional hologram is illustrated in figure 2.1. The light from a laser is divided into two separate beams by a beam splitter. A beam illuminates the object, the so called object beam, and is scattered and reflected onto whatever recording medium is being used. The reference beam is directed at the recording medium without being distorted in any way. To recreate a picture of the object the hologram is illuminated by the reference beam as in figure 2.2.

If the hologram has been created successfully the observer will see an image identical to the original object - an image much resembling the image one would see in a mirror, with depth of focus and three-dimensional properties.
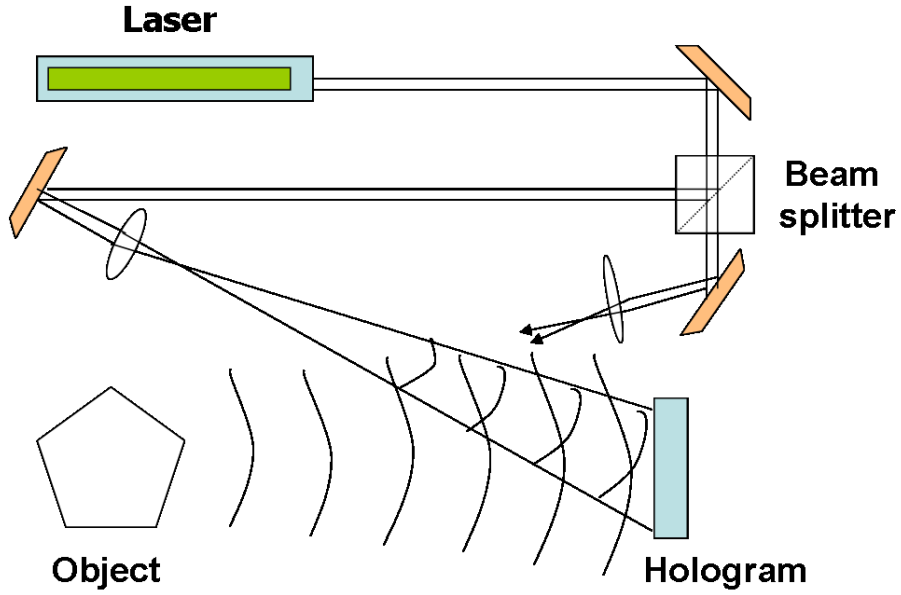
Figure 2.1: Construction of a hologram.

Formalising the description of holography;
The complex amplitude of the object wave and the reference wave are written as:

$$O(x, y) = o(x, y)e^{i\varphi_o(x,y)} \tag{2.1}$$

$$R(x, y) = r(x, y)e^{i\varphi_r(x,y)} \tag{2.2}$$

where o and r are the real amplitudes and φ_o and φ_r are the phases. These two waves will interfere and the resulting intensity in the plane of the hologram is:

$$
\begin{aligned}
I(x, y) &= |O(x, y) + R(x, y)|^2 \\
&= R(x, y)R^*(x, y) + O(x, y)O^*(x, y) \\
&+ O(x, y)R^*(x, y) + R(x, y)O^*(x, y) \\
&= |R|^2(x, y) + |O|^2(x, y) + O(x, y)R^*(x, y) + R(x, y)O^*(x, y)
\end{aligned}
\tag{2.3}
$$

with * denoting the complex conjugate. The amplitude transmission function $h(x, y)$ is proportional to the intensity and can be written as:

$$h(x, y) = h_0 + \beta\tau I(x, y) \tag{2.4}$$

where β is a constant, τ is the exposure time, and h_0 is the amplitude transmission function of an unexposed photographic plate. The reconstruction of the hologram is done by multiplying the amplitude transmission function with the reference wave:

$$
\begin{aligned}
R(x, y)h(x, y) &= [h_0 + \beta\tau(r^2 + o^2)]R(x, y) \\
&+ \beta\tau r^2 O(x, y) + \beta\tau R^2(x, y)O^*(x, y)
\end{aligned}
\tag{2.5}
$$

4
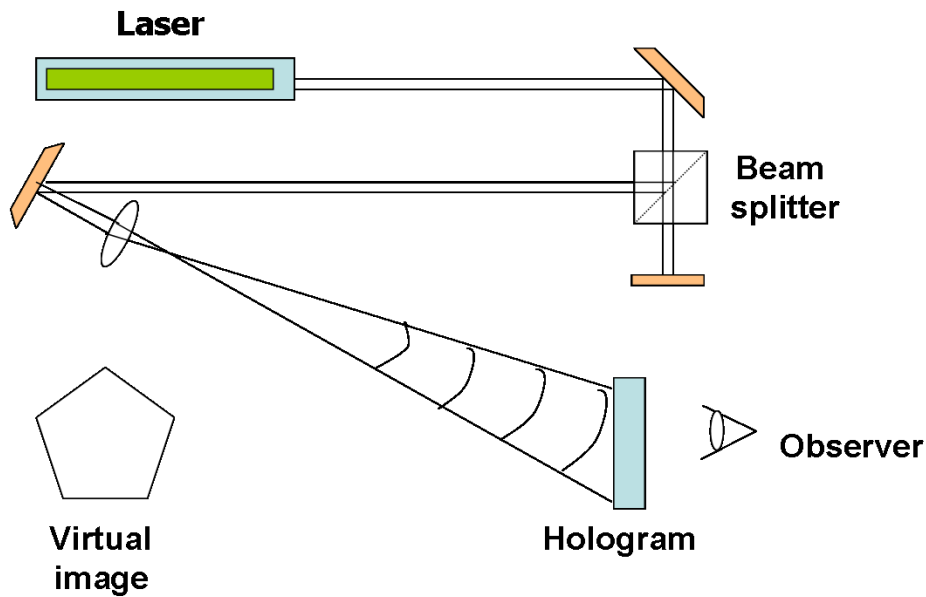
Figure 2.2: Reconstruction of a hologram.

The first term is the undiffracted reference wave, the second is the reconstructed object wave, and the third is a distorted real image of the object. In digital holography it is possible to record the reference wave and the object wave separately with a CCD. Therefore the intensity pattern originating from the two respective beams can be subtracted before processing the image. Hence the undiffracted reference wave will not contain the terms r^2 and o^2 which are included in the first term on the right hand side of equation 2.5. The logic of this reasoning may be found more accessible by consulting equation 2.3 [4][5]. Equivalent deductions can be found in Schnars and Jüptner [6] and Gustafsson et al [7].

Since this kind of holography is carried out with two separated beams the setup is very sensitive, especially to vibrations. On the other hand, when successfully carried out holograms will exhibit both depth of focus and effects of perspective. Furthermore, although the sensitivy very well can be a problem it also can turn out to be very useful. Interferometric holography is one example of holographic applications drawing on the sensitivity of the setup [5].

2.3 In-Line Holography

In-Line holography is based on Gabor's original idea of holography. In this form of holography the hologram is created by only one beam. The setup is similar to Young's famous experiment with a double slit – a beam is directed at an object and the interference is recorded at a plane behind the object. Since the beam is divergent the interference pattern will be subjected to geometric magnification. The setup is illustrated in figure 2.3.

The single beam, although bringing stability to the setup, also means complications.
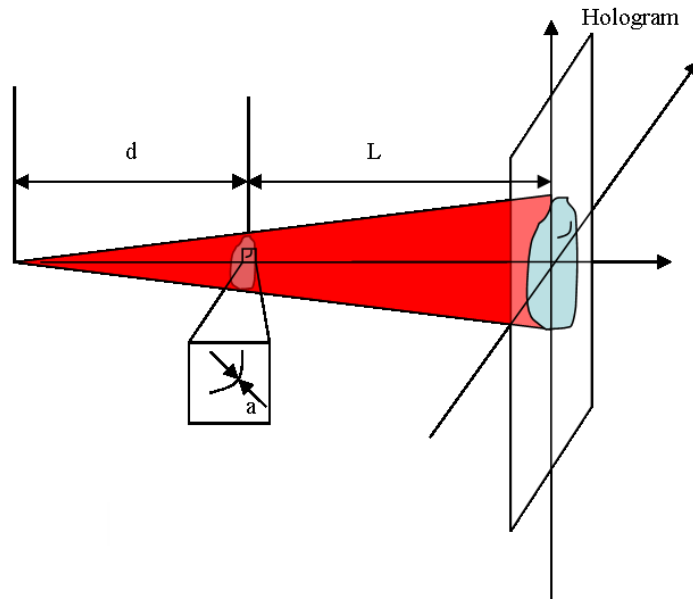
Figure 2.3: Setup for inline holography

The main complication is that the reconstructed object and the distorted real image of the object, the second and the third term on the right of equation 2.5, are aligned from the viewers point of view when reconstructing the image. In conventional holography the angle between the beams causes the images to look separated. This is illustrated schematically in figure 2.4. Since the images are in line in in-line holography there will be an out of focus image superimposed on the in focus image after the reconstruction. Gabor himself identifies the problem as that of the hologram effectively functioning as a Soret-lens, which is a lens that at the same time functions as a positive and a negative lens [3]. That is the key to interpreting figure 2.4. The virtual[1] images appear to be situated in front of the hologram and the real images appear to be behind. In the in-line case it is impossible to isolate one from the other. One way of viewing it is that the real image will have an out of focus virtual image superimposed when reconstructed. The virtual image will be out of focus by $2L$.

Although the problem cannot be fully solved in in-line holography, it can be contained. The most practical way is to make sure the object is small. By small is meant that it should only block a fraction of the radiation cone recorded on the screen [8]. The formal constraint is that the lateral dimension of the object should be small enough to fulfill the Fraunhofer condition:

$$a^2 \ll \lambda \cdot d \tag{2.6}$$

where λ is the wavelength of the recording beam and d is the distance between the object and the focus of the beam [9]. A similar approach to the problem is done by Koren et al. who simply set the constraint that the absorption should be a small fraction

---

[1]The terms virtual and real are somewhat arbitrary. Although the intensity of the images may not be the same, they both contain all relevant information. Thus the choice of which image is which is more down to preference and precedence than anything else.
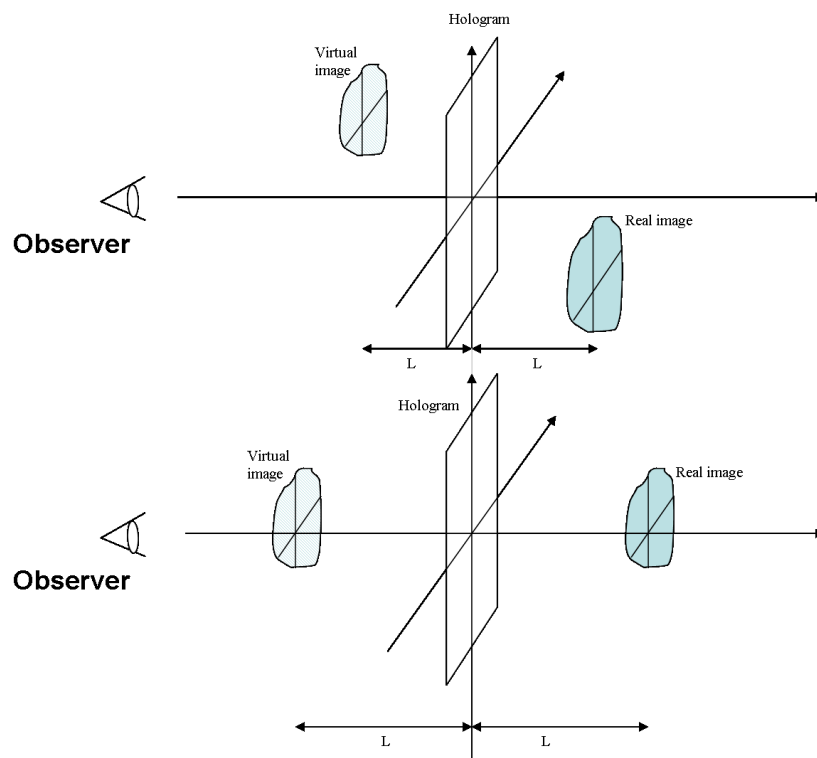
Figure 2.4: Schematic figure of how the images are seen in conventional (top) and in-line (bottom) holography

of the total [10]. Also, when the object only blocks a small part of the radiation cone, the reference beam subtracted by the hologram leads to a small 'twin image' term.

2.4 The Reconstruction Algorithm

Reconstructing an image is a process based on the Huygens-Fresnel principle. The principle states that every point in Plane 1 is the source of a spherical wavelet. Through superpositioning the wavelets from every point in Plane 1 the wave front in Plane 2 can be determined (figure 2.5)
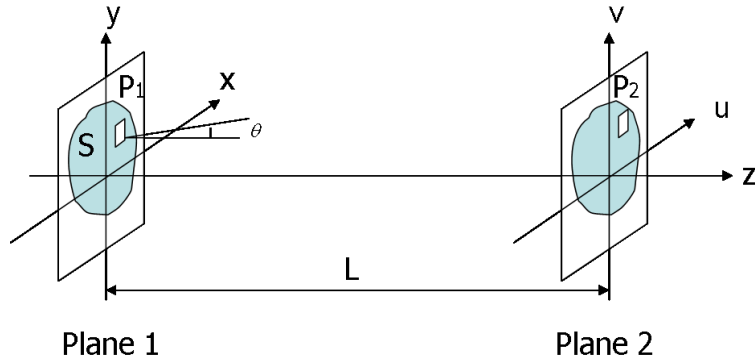
Figure 2.5: Notations for the Fresnel-Kirshoff integral

A mathematical realisation of this statement starts off with the Fresnel-Kirchoff integral:

$$E_2(u,v) = \frac{i}{\lambda} \cdot \int_S E_1(x,y) \cdot \frac{e^{-ikr}}{r} \cdot cos\theta dxdy \qquad (2.7)$$

where r is the distance from the point P_1 to the point P_2 in figure 2.5, θ is the angle between that line and the normal to the planes, and $E_1(x,y) \cdot \frac{e^{-ikr}}{r} dxdy$ is the spherical wavelet emanating from the area element $dxdy$. S is the area over which the integral is carried out.

Assuming that the paraxial approximation is valid, ie. $|u - x|, |v - y| \ll L$, or in other words that θ is small and $cos\theta \simeq 1$:

$$r = \sqrt{L^2 + (x-u)^2 + (y-v)^2} = L \cdot \sqrt{1 + \frac{(x-u)^2}{L^2} + \frac{(y-v)^2}{L^2}}$$

$$\approx L \cdot (1 + \frac{(x-u)^2}{2L^2} + \frac{(y-v)^2}{2L^2}) = L + \frac{(x^2+y^2)}{2L} + \frac{(u^2+v^2)}{2L} - \frac{(xu+yv)}{L} \quad (2.8)$$

and also introducing:

$$F_1^L(x,y) = E_1(x,y) \cdot e^{-ik \cdot \frac{x^2+y^2}{2L}} \qquad (2.9)$$

makes it possible to rewrite $E_2(u,v)$ as:

$$E_2(u,v) = \frac{i}{\lambda L} \cdot e^{-ikL} e^{-ik \cdot \frac{u^2+v^2}{2L}} \int_S F_1^L(x,y) e^{ik \cdot \frac{xu+yv}{L}} dx dy$$

$$= \frac{i}{\lambda L} \cdot e^{-ikL} e^{-ik \cdot \frac{u^2+v^2}{2L}} \cdot \tilde{F}_1^L \left(\frac{ku}{2\pi L}, \frac{kv}{2\pi L} \right) \tag{2.10}$$

where $\tilde{F}_1^L$ is the Fourier transform of F_1^L. Often this equation can be found with the opposite signs in the exponents. That is simply due to the choice of the direction of r.

Assume three planes, the object plane, the hologram plane, and a far field plane as in figure 2.6. The electrical field in the far field plane can then be determined by knowing what it looks like in every single point of any of the two other planes respectively:
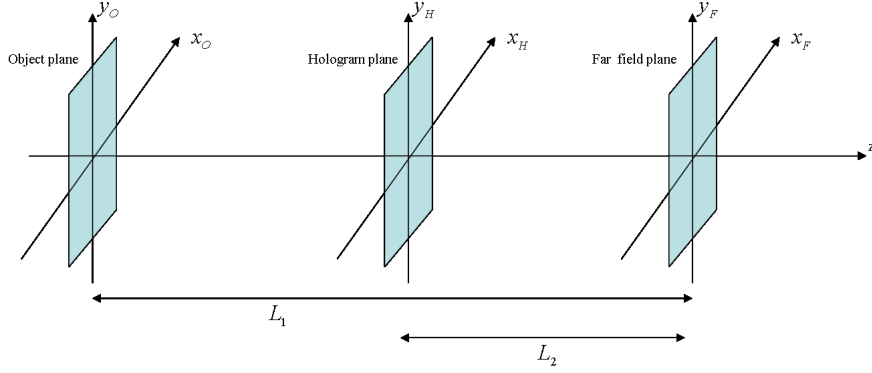
Figure 2.6: Three planes.

$$E_F(x_F, y_F) = \frac{i}{kL_1} \cdot e^{-ikL_1} e^{-ik \cdot \frac{x_F^2+y_F^2}{2L_1}} \cdot \tilde{F}_O^{L_1} \left(\frac{kx_F}{2\pi L_1}, \frac{ky_F}{2\pi L_1} \right) \tag{2.11}$$

$$E_F(x_F, y_F) = \frac{i}{kL_2} \cdot e^{-ikL_2} e^{-ik \cdot \frac{x_F^2+y_F^2}{2L_2}} \cdot \tilde{F}_H^{L_2} \left(\frac{kx_F}{2\pi L_2}, \frac{ky_F}{2\pi L_2} \right) \tag{2.12}$$

Since the left hand sides of both equations are equal:

$$\tilde{F}_O^{L_1} \left(\frac{kx_F}{2\pi L_1}, \frac{ky_F}{2\pi L_1} \right) = \frac{\frac{i}{kL_2} \cdot e^{-ikL_2} e^{-ik \frac{x_F^2+y_F^2}{2L_2}}}{\frac{i}{kL_1} e^{-ikL_1} e^{-ik \cdot \frac{x_F^2+y_F^2}{2L_1}}} \cdot \tilde{F}_H^{L_2} \left(\frac{kx_F}{2\pi L_2}, \frac{ky_F}{2\pi L_2} \right)$$

$$= \frac{L_1}{L_2} \cdot e^{-ik(L_2-L_1)} e^{-ik \frac{x_F^2+y_F^2}{2} \left(\frac{1}{L_2} - \frac{1}{L_1} \right)} \cdot \tilde{F}_H^{L_2} \left(\frac{kx_F}{2\pi L_2}, \frac{ky_F}{2\pi L_2} \right) \tag{2.13}$$

From which the electrical field in the object plane is isolated leading to the equation:

$$E_O(x_O, y_O) = e^{+ik \cdot \frac{x_O^2 + y_O^2}{2L_1}}$$
$$\cdot FT^{-1} \left\{ \frac{L_1}{L_2} \cdot e^{-ik(L_2 - L_1)} e^{-ik\frac{x_F^2 + y_F^2}{2}(\frac{1}{L_2} - \frac{1}{L_1})} \cdot \tilde{F}_H^{L_2}\left(\frac{kx_F}{2\pi L_2}, \frac{ky_F}{2\pi L_2}\right) \right\}$$

$$(2.14)$$

which is the recipe for reconstruction in in-line holography. Similar derivations to the one carried out here can be found in [11][12]. It is also possible to arrive at an equivalent solution through a convolution approach which is done by [7].

There is one major obstacle that cannot be overcome in digital holography. When the hologram is recorded it is the intensity that is recorded. Therefore the reconstruction of the object will have to be made with $\sqrt{I_H(x_H, y_H)}$ instead of $E_H(x_H, y_H)$, which of course entails a loss of phase information. This leads to the reconstruction formula which actually is implemented:

$$E_O(x_O, y_O) = e^{ik \cdot \frac{x_O^2 + y_O^2}{2L_1}}$$
$$\cdot FT^{-1} \left\{ \frac{L_1}{L_2} \cdot e^{-ik(L_2 - L_1)} e^{-ik\frac{x_F^2 + y_F^2}{2}(\frac{1}{L_2} - \frac{1}{L_1})} \cdot \tilde{G}_H^{L_2}\left(\frac{kx_F}{2\pi L_2}, \frac{ky_F}{2\pi L_2}\right) \right\};$$

$$(2.15)$$

where $\tilde{G}_H^{L_2}$ is similar to $F_H^{L_2}$ except that E_H is replaced by $\sqrt{|E_H|^2}$ in the Fourier transform. To recover the phase information, an iterative process can be implemented. The reconstructed object is simply used to simulate a new hologram. This is done through using equations 2.11 and 2.12 to isolate the electrical field in the hologram plane, leading to:

$$E_H(x_H, y_H) = e^{ik \cdot \frac{x_H^2 + y_H^2}{2L_2}}$$
$$\cdot FT^{-1} \left\{ \frac{L_2}{L_1} \cdot e^{-ik(L_1 - L_2)} e^{-ik\frac{x_F^2 + y_F^2}{2}(\frac{1}{L_1} - \frac{1}{L_2})} \cdot \tilde{F}_O^{L_1}\left(\frac{kx_F}{2\pi L_1}, \frac{ky_F}{2\pi L_1}\right) \right\}$$

$$(2.16)$$

The intensity of this hologram is replaced at every point with the intensity of the original hologram. This matrix will now contain a first guess at the phase information of the hologram and a correct intensity at every point. This educated guess of a hologram is used to reconstruct the object again through equation 2.14. This process is to be carried out until the results are satisfactory. This particular method is described and implemented in [11]. The implementation of the algorithm was attempted, but the attempts were unfortunately unsuccessful. Equation 2.16 is however exactly how the holograms in the simulation below are created, and the recreation of the objects is of course done by equation 2.15. Further, we found that the recreation of the objects using only one iteration (2.15), in our case provided very satisfactory results

2.5 Reconstruction Programs for Digital Holography

Apart from having written a program during the diploma thesis I have also had two other programs at my disposal. Both programs are programs for conventional digital holography. They have both been used to verify and confirm the results obtained with my own program. One of the programs has been created by Sven-Göran Pettersson and the other by Mats Gustafsson. Since these programs have been constructed for conventional holography slight modifications have been made to accomodate for differences in the reconstruction process of Digital In-Line holography. In concrete terms; in conventional digital holography three pictures are taken, one reference picture, one object picture, and one hologram. The two first pictures are then subtracted from the third, as mentioned in the section on Conventional Holography. In Digital In-Line Holography the object picture does not exist. The way of modifying the programs for this has simply been to replace the object picture with a matrix of zeros. In the case of Mats Gustafsson's program the code was accessible to me and I also made a few adjustments to make it more user friendly from an in-line point of view.

2.6 Simulations

Equation 2.14 has been implemented in Matlab and is the foundation of the digital holography recreation process. However, before implementing the code on actual objects, a simulation has been carried out. The aim of the simulation is to determine how different parameters affect the reconstruction of the object. Those parameters are; the shape of the object, the frequency, and the distance between the object and the hologram. Finally, the simulation has also been carried out with several frequencies simultaneously, in order to simulate the reconstruction process with high harmonics.

Since the effect of the shape and size of the object is not fully known prior to the simulation, an object with straight lines, curves and variable lateral dimension is chosen – a comic strip (figure 2.7). The quality of the comic strip in the figure is of the same quality as the picture used in the algorithm, 256x256 pixels and in black and white. In the object plane the comic strip will be superimposed by a plane wave with a Gaussian profile (figure 2.8).

2.6.1 Simulation with One Harmonic

In figure 2.9 the distance between the hologram and the object is varied. The simulated wavelength is $\frac{800}{7} \approx 114$ nm, the pixel size 10 μm, and $\omega_0 = 2100$ μm (ω_0 is the radius from the intensity peak of the beam at which the intensity of the Gaussian has decreased to $\frac{1}{e^2}$). As expected the likeness to the object of the hologram decreases as the distance between the object and the hologram increases. Image A is somewhat similar to the original object while image G bears little resemblance. This does, however, not seem to have any effect whatsoever on the reconstructed object. The details of the object appear equally well in all the reconstructed images. There is a marked difference between the reconstructed images though. In image B there are clear disturbances around the recreated object that are not visible in the other reconstructions. These are most likely due two the twin image phenomenon. Since image B is recreated from a hologram only 5 cm from the object, the out of focus image superimposed would be 10 cm out of focus. By comparing image B to image C – which apart from being a hologram also can be viewed as an out of focus image of the object at a distance of
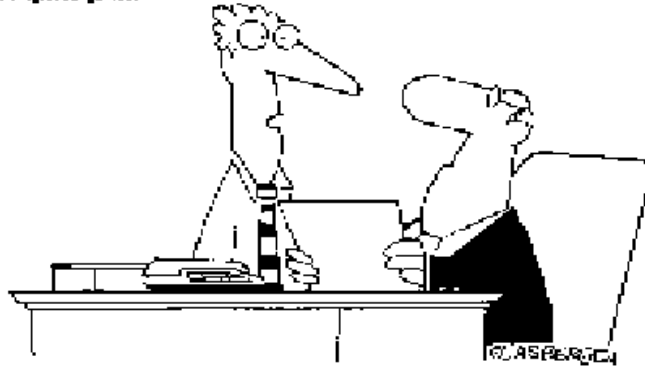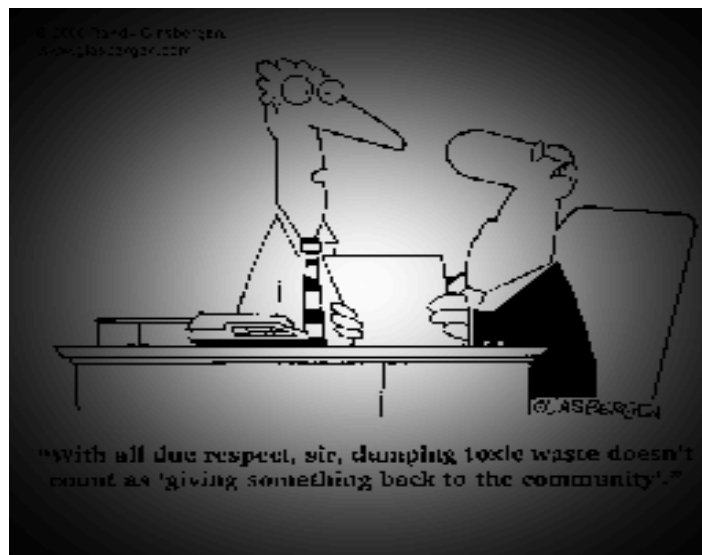
Figure 2.7: Comic strip

Figure 2.8: The comic strip superimposed with a gaussian profile

10 cm – the assumption is corroborated. Further affirmation is sought by simulating a holographic reconstruction at a distance of 1 cm. As seen in figure 2.10 B the assumed twin image superimposed bears even more resemblance of the original object than previously, hence the twin image assumption is further ascertained.

A pattern much resembling a frame becomes more and more evident in the pictures as the distance increases. This phenomenon seems to arise in conjunction with straight lines in the picture and especially the borders of the picture. Comparing the simulated holograms with the reconstructed images it is evident that the occurence is present in both, though clearer in the reconstructed images. This leads to the conclusion that it has something to do with the Fast Fourier Transforms carried out in the algorithm. One hypothesis is that reducing the values around the borders of the picture will reduce the framing effect. Therefore the simulation in figure 2.11 has been carried out with $\omega_0 = 1400$. However, there is no visible improvement. Also filtering has been tried to surmount the problem, but without success. It turns out the quality of the actual reconstructed object is deteriorated if the frames are to be dealt with in that way.

The problem of the frames does not necessarily have to be overcome. It can be regarded as merely an aestetic nuisance since it does not seem to impose on the reconstructed image in any way. Furthermore, when the program is run on real holograms, the frames will not be present in the holograms. Hence the effect should only occur to the extent it occurs in the simulated holograms. One way of forcing oneself around the problem with the frames is to record a hologram without an object and recreate it. The recreated object can then be subtracted from that image. Since both images contain the same defects the problem is overcome. This method results in the final image being inverted in appearance and requires a stable source of light should it be carried out. Tests have shown [8] that even the stability of a laser pointer will suffice.

The effect of different wavelengths was also simulated. Figure 2.11 illustrates the effects of various wavelengths. The distance between the object and the simulated holograms is 40 cm, the sampling distance is 10μm, and $\omega_0 = 1400$. Lowering the wavelength has the same effect as the shortening the distance. The similarity between the hologram and the original object increases as the wavelength decreases. The problem with the frames does not seem to impose more on the recreated picture as the wavelength is decreased. However the frames tend to appear closer to each other. As previously, the reconstruction quality of the object does not seem to suffer from the usage of higher harmonics.

2.6.2 Simulation with Several Harmonics

This is the final step of the simulation. So far the relevant aspects of the reconstruction process have been covered. However, when performing the holographic experiment with high order harmonics there will arise further problems. Although spectral filtering will be used to single out a few harmonics, there will still be several harmonics present when the hologram is recorded. In order to ascertain the effects of this a simulation has been made. Throughout the simulation with several harmonics all harmonics have been assumed to have the same intensity. The simulated holograms are created according to the following formula:

$$E_H(x, y) = \sum_n E_H^{2n+1}(x, y); n \in N \tag{2.17}$$

The reconstruction is made according to the same principle. However since the phase information will be lost in the experimental case the square root of the modulus of the

amplitude will be used.

Figure 2.12 displays the effect of creating a hologram and recreating the object with all harmonics up to the 23:rd. Clearly the reconstruction is severely blurred. This is not unexpected. The reconstruction with several harmonics is the same as reconstructing with one harmonic at a time and subsuquently adding the pictures. Every such reconstruction would recreate the object slightly differently, thus creating a blurred image. However reconstructing the object with only one harmonic does not improve matters. As shown in figure 2.13 the reconstructed object instead appears faint, although what little can be observed of it does seem rather less blurred than figure 2.12 B. For example a hint of the pattern of the clerks tie can be seen. This concurs with the previous reasoning. This reconstruction can be viewed as one of the several which form figure 2.12 B.

Luckily spectral filtering will remove all harmonics up to the 13:th [2]. Thus the experimental hologram will be created with three or four harmonics. This has been simulated in figure 2.14. The hologram is created with four harmonics and the reconstruction is made with one of the harmonics in B, and all four of the harmonics in C. Reconstruction C does seems to be of higher quality, however this may well be due to destructive interference of the frames. The reconstructed objects seem to be of comparable quality.

---

[2]More on this can be found in the following chapter
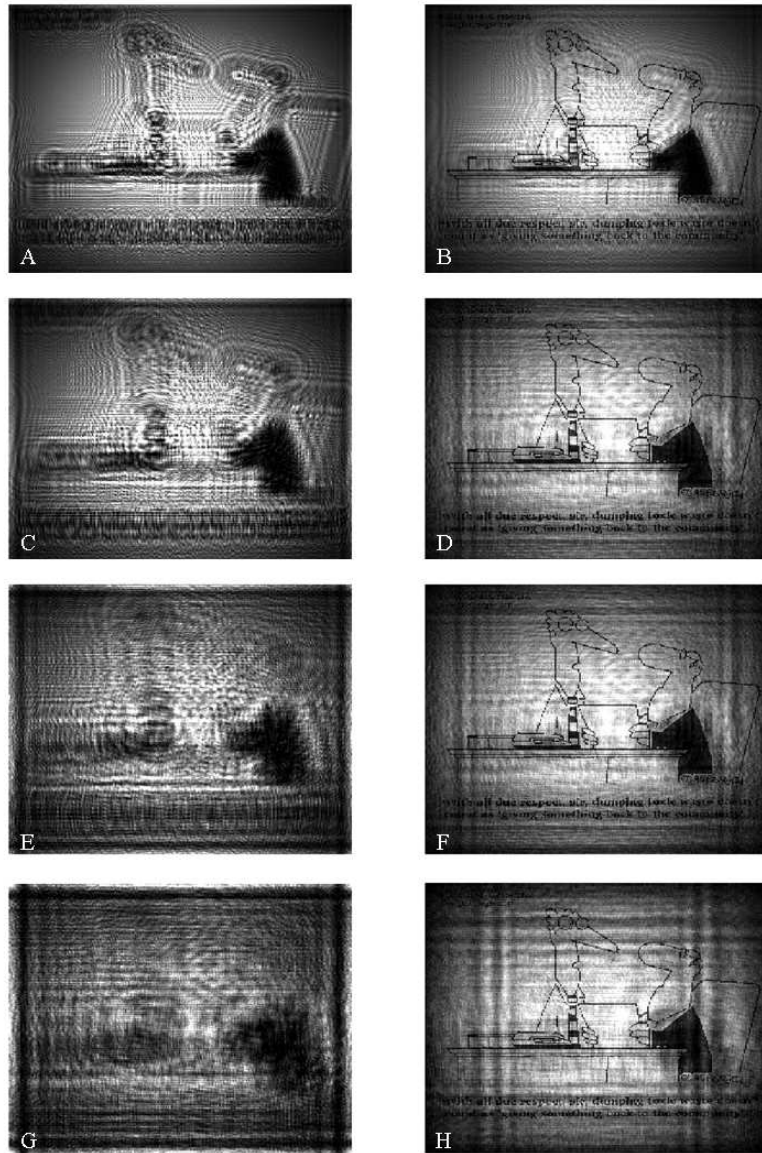
Figure 2.9: Variation of the distance between the object and the simulated hologram. The wavelength is 800/7 nm, i.e. the 7:th harmonic. The holograms are in the left column and the reconstructions in the right. A,B: distance 5 cm. C,D: distance 10 cm. E,F: Distance 20 cm. G,H: distance 40 cm
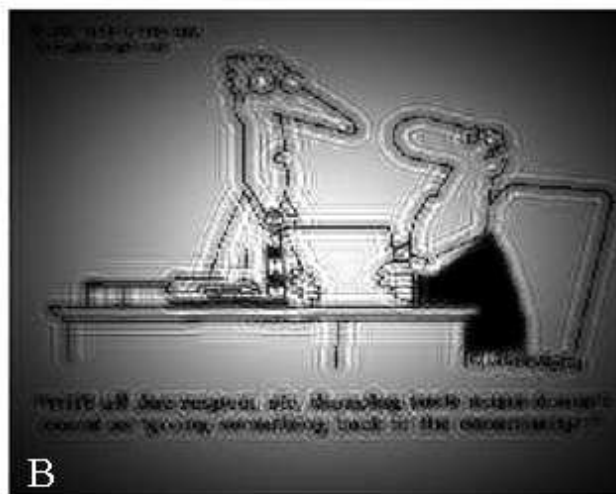
Figure 2.10: A: The simulated hologram. B: The reconstructed object. Distance 1 cm.
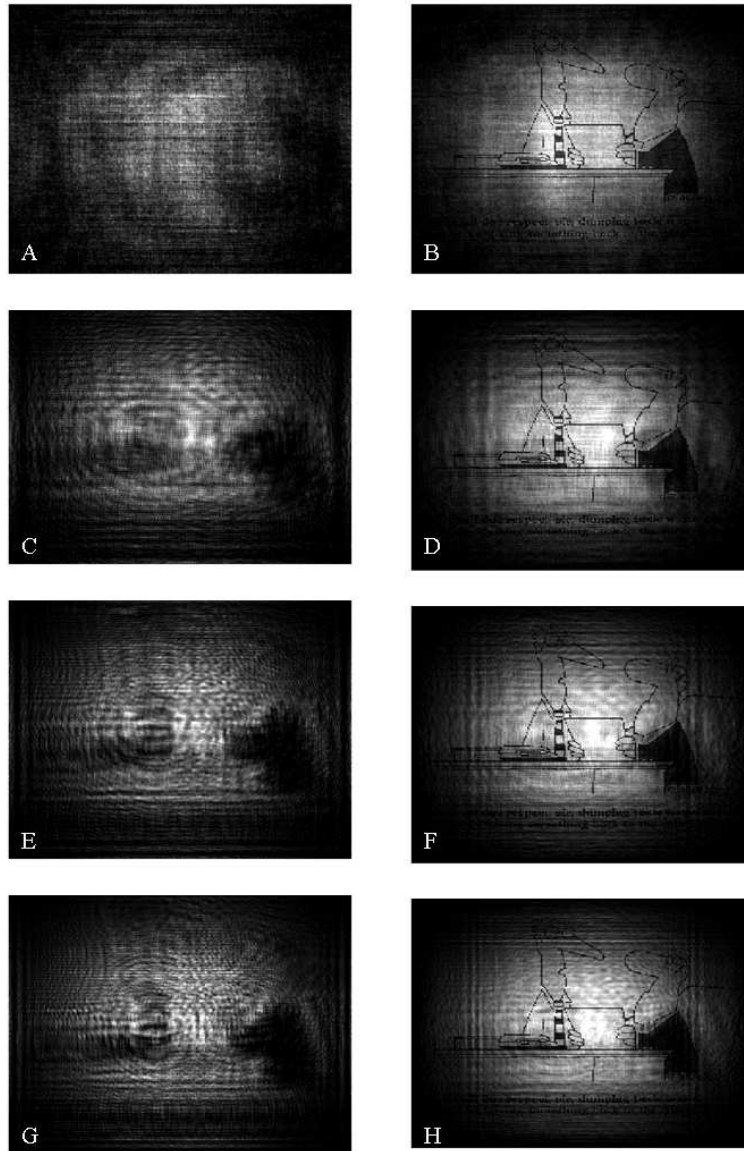
Figure 2.11: Variation of the wavelength. The holograms are in the left column, the reconstructions in the right. A,B: fundamental. C,D: 7:th harmonic. E,F: 13:th harmonic, G,H: 19:th harmonic

17

Figure 2.12: Simulated hologram and reconstructed object created with odd harmonics 1-23.

Figure 2.13: Reconstructed object created with harmonic 11. Hologram created with odd harmonics 1-23.
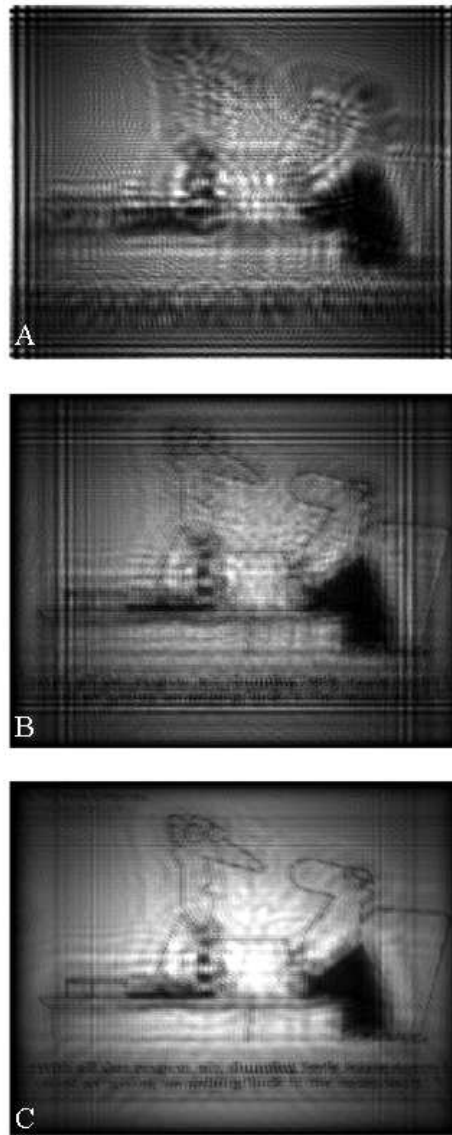
Figure 2.14: A: Simulated hologram. B: Reconstructed object created with harmonic 19. C: Reconstructed object created with odd harmonics 17-23.

Chapter 3

Harmonic Generation

3.1 The principle of High Harmonic Generation

The three step model, also known as the semi-classical model of high harmonic genera-
tion, provides a fairly intuitive understanding of the high harmonic generation process.
In this model the atom is approximated to have only one electron. The motion of this
electron in the laser field is treated classically while the active tunneling and recombi-
nation processes are treated quantum mechanically.

Since the electric field strength created by the laser when generating harmonics is
close to the electric field experienced by the electron in the Coulomb potential, the
Coulomb potential will be severely distorted. The electrical field experienced by the
electron in the ground state of a hydrogen atom is $5 \cdot 10^9$ V/cm The laser intensity I
which genererates that electrical field strength E can be calculated through:

$$I = \frac{1}{2}\epsilon_0 c |E|^2 \tag{3.1}$$

where ϵ_0 is the electrical permitivity of vacuum and c the speed of light. This leads to
an intensity of $3.5 \cdot 10^{16}$ W/cm^2 which is not far from the 10^{14} W/cm^2 used for high
harmonic generation. The distorted potential will take the shape shown in figure 3.1,
which is generally referred to as the tunnel ionisation regime.
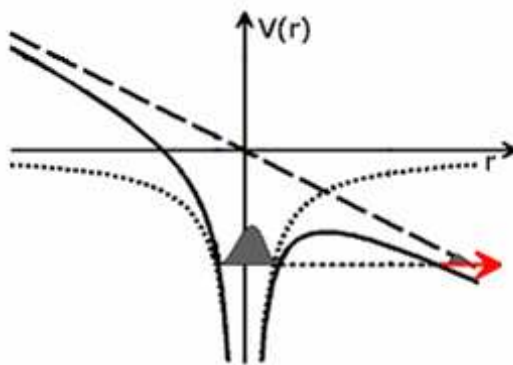
Figure 3.1: Tunnel ionisation [13].

The three steps of The Three Step Model of harmonic generation are illustrated in figure 3.2 and can be summarised by:

i The atom is ionised through the tunnel ionisation process.

ii The electron is accelerated away from the atom by the electric field. When the field changes the electron is accelerated in the opposite direction, back towards the atom.

iii When the electron is close to the atom there is as certain probability of recombination back to the ground state. The liberated energy of the electron is emitted as a photon.
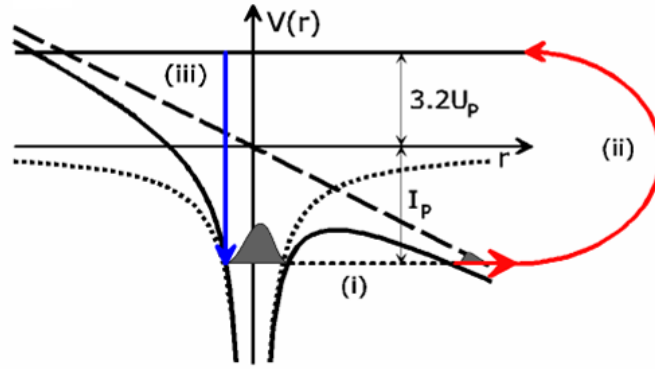
Figure 3.2: The three step model [13].

The model implies that the laser light needs to be linearly polarised. Otherwise the electron would not be accelerated back towards the atom with a significant probability. The process occurs twice each laser period and it is possible to calculate the trajectory of the electron and hence the kinetic energy at the time of recombination. The calculation is done with the Newtonian equation of motion with the condition $x_t(t) = 0$, where t_t is the tunneling time. The results lead to the maximum harmonic cutoff energy giving:

$$E_f = I_p + 3.2U_p \qquad (3.2)$$

where I_p is the ionisation potential of the electron [13][14][15].

3.1.1 Phase Matching and Focusing Conditions

In order to allow for an efficient transfer of energy from the fundamental field to the harmonic field it is vital that phase matching is achieved. Among other things this is done by loose focusing geometry. This is because there is a phase shift of 180 degrees – Gouy phase shift – at the focus of a beam. By focusing the beam with a lens with a relatively long focal length this effect will be less dramatic. Also the necessary intensity

for High Harmonic Generation will be maintained over a larger region of space. The radius of a Gaussian beam is defined by:

$$w_0 = \frac{\lambda f}{\pi w} \tag{3.3}$$

where f is the focal length of the lens and w is the original radius of the beam. The length of the focal region which is defined as the region within which the beam area is less than twice the area of the beam at the beam waist is:

$$2 \cdot z_R = \frac{\pi w_0^2}{\lambda} = \frac{\lambda f^2}{\pi w^2} \tag{3.4}$$

where z_R is the Rayleigh distance.

3.2 Experimental Setup

The setup for Harmonic generation is relatively simple. The laser pulse is focused in a gas medium. The laser beam and the harmonics are separated by a spectrometer and the harmonics are detected. The setup is illustrated in figure 3.3 below. This section will be divided into several subsections addressing the various components of the setup.
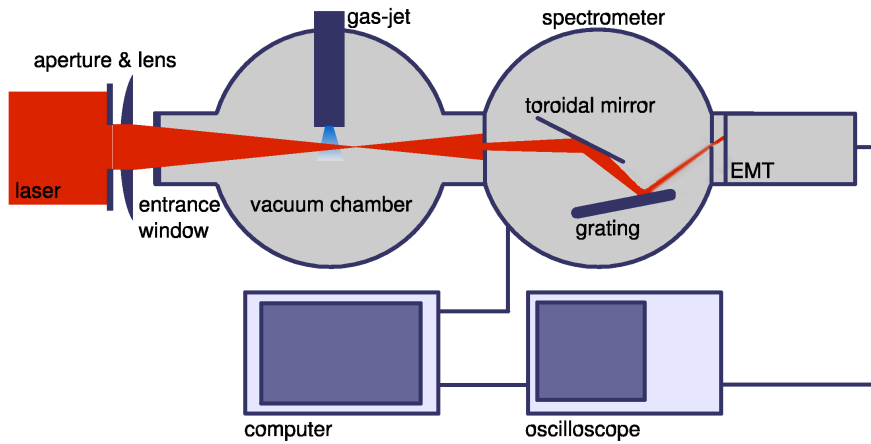
Figure 3.3: Principle setup for harmonic generation [15].

3.2.1 The Laser

Harmonic generation is done with laser pulses from the terawatt laser at the Lund High-Power Laser Facility at the Lund Laser Centre (LLC). The laser is a Ti:sapphire laser and the pulses are amplified by the chirped pulse amplification technique. The system delivers ten pulses per second at 800 nm, pulses which are approximately 35 fs each. The beam diameter is approximately 4 cm at $(1/e^2)$ and the pulse energy is roughly 100 mJ when it reaches the harmonic setup.

3.2.2 The Vacuum System

The vacuum system is pumped by two pump setups each consisting of a turbo pump and a rotary pump. One pump system pumps directly under the gas jet in order to minimise the deterioration of the vacuum due to the gas releases. The other is placed adjacent to the EMT (Electron Multiplier Tube), which is the component of the setup which requires the lowest pressure to function. The pressure during harmonic characterisation was around 10^{-4} mBar in the gas chamber and 10^{-5} mBar by the EMT.

3.2.3 The Gas Medium

The gas supply to the setup comes from a tube of Argon gas. The noble gases are the most suitable elements to use for harmonic generation and Argon provides a spectrum suitable to the ends of this thesis. The Argon gas is fed through a tube in which it is contained at a chosen backing pressure. Ten times per second the gas is let out into the harmonic generation chamber in one millisecond bursts. With the aid of an oscilloscope the bursts are set so that they end at the same instant the laser pulse arrives; that way the loss of vacuum is minimised while optimising the amount of gas for the laser pulse to interact with. These settings were done with a delay generator triggered by the laser system.

3.2.4 Focusing

As noted previously loose focusing is beneficial for harmonic generation. In order to optimise the focusing conditions a combination of an aperture and a lens is used. The aperture (figure 3.3) is used to vary the diameter of the beam let into the setup and, of course, the intensity. The lens, which has a focal length of one meter, is carefully placed on a meticulously aligned rail. Thus the lens can be moved back and forward along the beam with the beam passing through its centre at every position.

3.2.5 The Spectrometer

The spectrometer used in the setup is a I.S.A. Jobin-Yvon PGM PGS 200. When arriving at the spectrometer, the fundamental and the harmonics travel along the same axis. Since the energy of the fundamental is several orders of magnitude larger than that of the harmonics they need to be separated. This is done in the spectrometer. The light passes through an adjustable entrance slit and is focused by a toroidal mirror onto a plane platinum grating. The grating has 450 grooves per millimeter and is designed for the spectral range 16 nm to 80 nm. The light is reflected by the grating onto a 150 μm wide exit slit; thus the entrance slit is imaged on the exit slit. Naturally, the narrow slits lead to the necessity of a painstakingly precise alignment, an arduous task which however is duly rewarded with a harmonic spectrum.

3.2.6 Data Acquisition

The principle setup for data aquisition is as in figure 3.4. The back reflection from the laser pulse as it enters the harmonic setup is used to trigger the diode. The signal from the diode is used to trigger the oscilloscope. Simultaneously the EMT, to which a voltage of 3000 V is applied, will register a signal which is seen on the oscilloscope. Initially a preampilifier was used between the EMT and the oscilloscope, however,

since it affected the signal in a negative way, it was removed. When proceeding without the preamplifier it is advisable to attach a resistor to the cable joining the oscilloscope to the EMT in order to protect the sensitive channels.
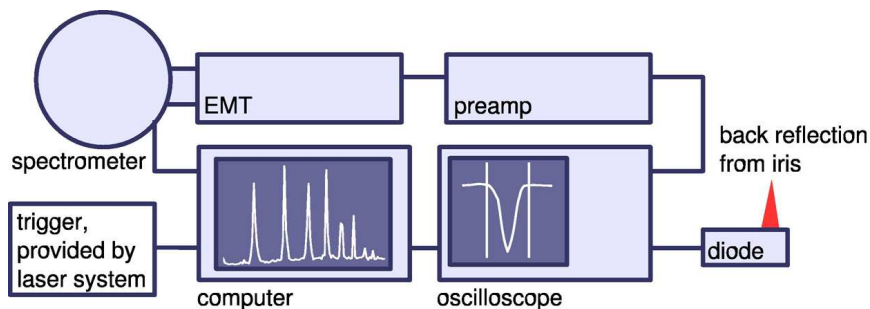

Figure 3.4: Principle Setup for data acquisition

The laser trigger pulse, which is connected to the computer via the delay box of the gas supply, triggers the computer program. At each incident pulse it integrates the voltage curve over a chosen time interval on the oscilloscope. The value of the integral is plotted versus the setting of the spectrometer by the program and is proportional to the number of registered photons by the EMT at the given position of the spectrometer.

3.3 Measurements and Optimisation

The process of optimising the harmonics is fairly intuitive and simple. Three different parameters are varied, one at a time, while everything else is kept constant. The parameters that will be varied are the aperture, the distance between the lens and the gas jet, and the backing pressure. The nature of the harmonics does seem to vary slightly on a day to day basis, which can be put down to the nature of the laser pulse entering the setup on a given day. Therefore a certain setting cannot be taken as the optimal setting simply because it was so the previous day. Every measurement has, of course, been preceded by checking the alignment of the beam and observing that the tell tale spark beneath the gas jet is present.

Before proceeding with the optimisation process it should be noted that a zero level was set based on the average value of a number of shots, usually 100. This screens out most of the background noise. However the background noise is affected differently by different parameters. It tends to be lower the further away the spectrometer is from the zeroth order and it tends to increase as the backing pressure is increased. Therefore the intensity in the following graphs will not necessarily have its minimum at zero, although it will be in the vicinity.

The displayed spectra all start at the 15:th harmonic. Some measurements are made up to the 23:rd harmonic and some to the 25:th. However the harmonics of main interest are the 17:th , the 19:th, and the 21:st since these are the ones which should dominate when the harmonics are used for holographic purposes.

3.3.1 Varying The Focal Point

First of all the focal point has been varied. This has been done with an aperture diameter of 12 mm and a backing pressure of 1 atm. The position of the lens that is indicated in the graphs in figure 3.5 is read from the translation rail that the lens is fastened to. The right edge of the unit holding the lens is the point used. Since the lens alledgedly has a focal length of one meter, the measurements start at that point, which is approximately equivalent to 340 mm on the translation rail. The lens positions have been indicated according to the translation rail since those measurements are far more exact.

By comparing the intensities of the different spectra in figure 3.5 it is evident that the most favourable lens position is either 350 mm or 360 mm. According to theory, the harmonic spectrum generated when the focus of the beam is exactly at the generation point, has slightly lower peak intensities than spectra generated just out of focus. There are no indications of this in the graphs in figure 3.5. Spectra were also taken at lens positions of 355 mm and 365 mm. But, as can be seen in figure 3.6 there is no clear indication of the exact position of the focus. However the three spectra at 350 mm, 355 mm, and 360 mm which have equal peak intensities, provide substance to the educated guess that the focus is between 350 mm and 360 mm. No real conclusions can be drawn from the internal distribution of the spectra, apart from the fact that placing the focus before the generation point seems to work to the relative advantage of the higher harmonics. When the lens is at 380 mm the 21:st harmonic is the most intense one in the spectrum.
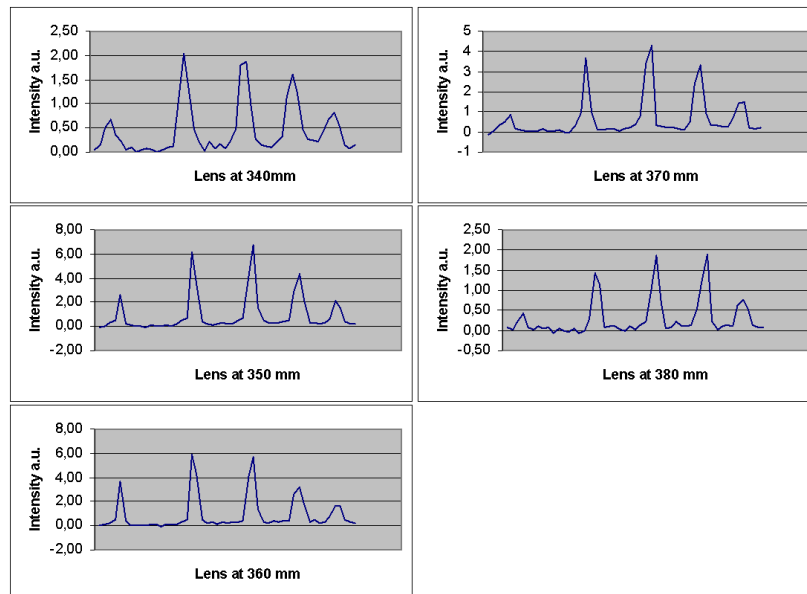

Figure 3.5: Harmonic spectra with different focal points

3.3.2 Varying The Aperture

In figure 3.7 the aperture is varied. The lens position is at 350 mm and the backing pressure is 1 atm. When the aperture is as little as 6 mm there is no visible harmonic
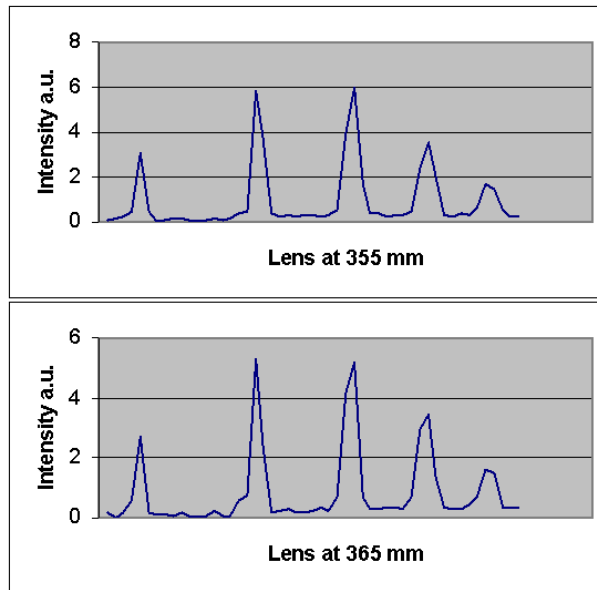
Figure 3.6: Harmonic spectra with different focal points

spectrum and when it reaches 16 mm the spectrum is hardly visible. It is clear that the ideal diameter of the aperture is in between. The four graphs displaying such apertures all show very clear harmonic spectra, whereas the spectra for apertures of 10 mm and 12 mm have the highest peak intensities.

3.3.3 Varying The Backing Pressure

In figure 3.8 the lens position is at 340 mm and the aperture is set at 14 mm while the backing pressure is varied. In retrospective the settings of these measurements are not quite the same as the optimal settings during the other measurements. The probable cause of this is that these measurements were made on another day than the previous ones and that the alignment of the laser prior to the setup for harmonic generation may have been slightly different. Later experiments further confirmed this hypothesis. However, the effects of the backing pressure on the harmonic spectrum should not be affected by this. As seen in figure 3.8 increasing the pressure above atmospheric pressure does not seem to entail any drastic change of the spectrum. Perhaps the intensity can be said to increase slighty, but the increase is not very large once compensated for the increase in background noise which comes with increased backing pressure. Lowering the backing pressure below atmospheric pressure however clearly lowers the peak intensities of the harmonics.
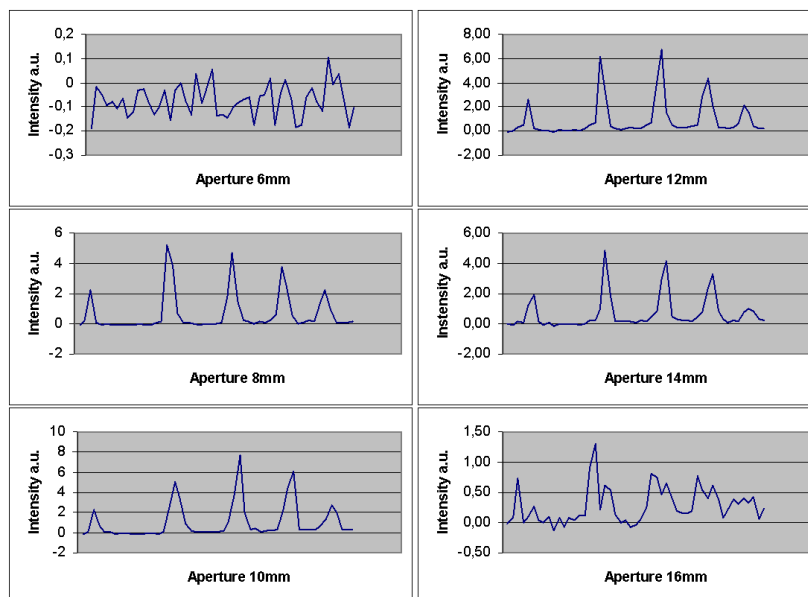
Figure 3.7: Harmonic spectra with different apertures.

3.4 Elimination of the fundamental and Spectral Filtering

Elimination of the fundamental and spectral filtering can both be achieved with an aluminium filter. The fundamental needs to be removed since it will not be spatially separated from the harmonics once the spectrometer is removed. Aluminium exhibits fairly good transmission in the wavelength region $20 - 60$ nm as illustrated in figure 3.9. The figure is plotted for a 200 nm aluminium filter, which is the thickness used is all experiments with a filter. The idea of the filter is that it reduces the number of harmonics.

The spectra that figure 3.10 is composed of are recorded with an aperture of 14 mm, the lens at 340 mm and the backing pressure at 1 atm. These were the best settings that could be found on the actual day. The procedure was to quickly optimise the setup without the filter and record a spectrum. Then the filter was inserted with the translation arm and the signal was maximised. After that the spectrum with the filter was recorded. As can be seen in figure 3.10 the filter reduces the 15:th harmonic to next to background level. This is not quite expected according to figure 3.9. The reason is that the filter is coated with a thin oxide layer which distorts the transmission profile. In figure 3.11 a graph over the properties of a filter equivalent to the one usesd here illustrates the discrepance. Still, the difference is not fully accounted for . A slight misalignment of the filter would most probably account for the rest of the difference. However, there are still four or five harmonics of very similar intensity. This could lead to a blurred holographic recreation according to the simulations in the previous chapter.
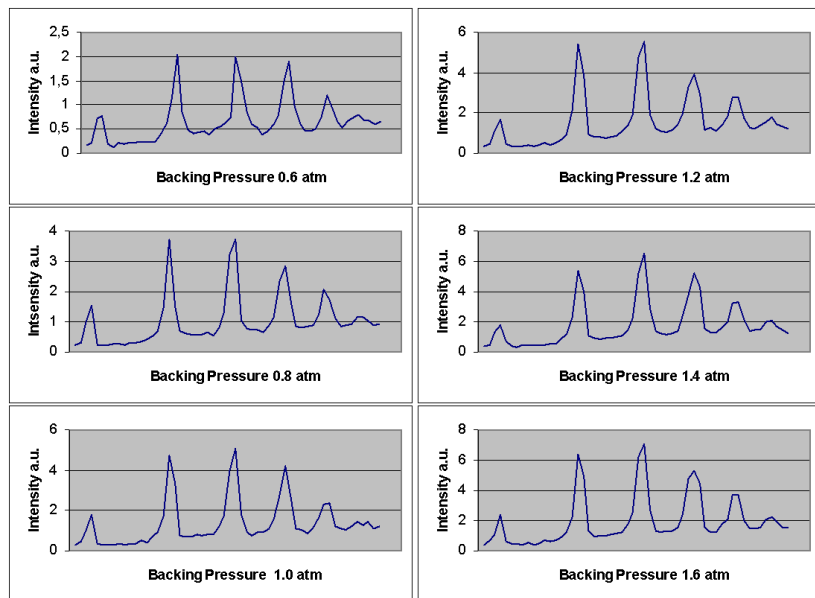
27

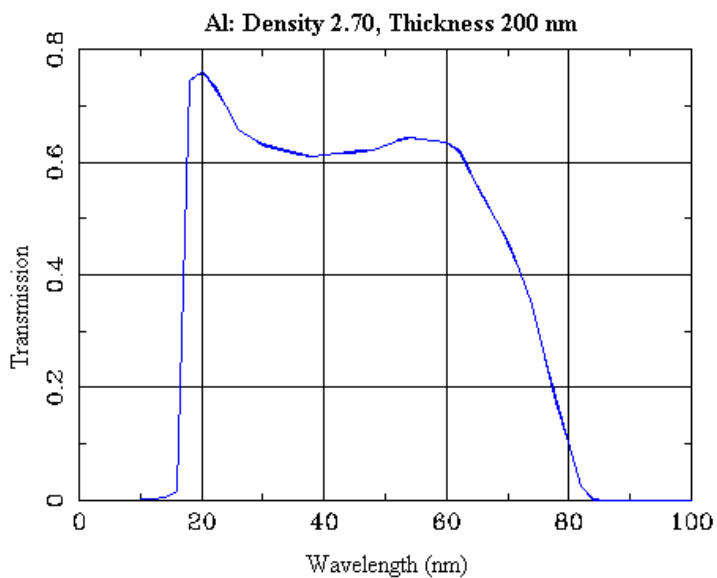Figure 3.8: Harmonic spectra with different backing pressures

Figure 3.9: Transmission of aluminium filter for different wavelengths
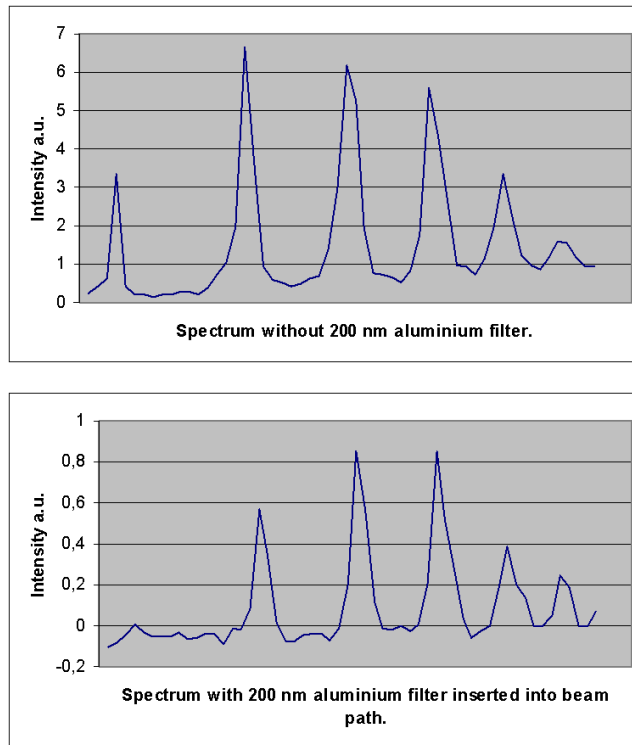
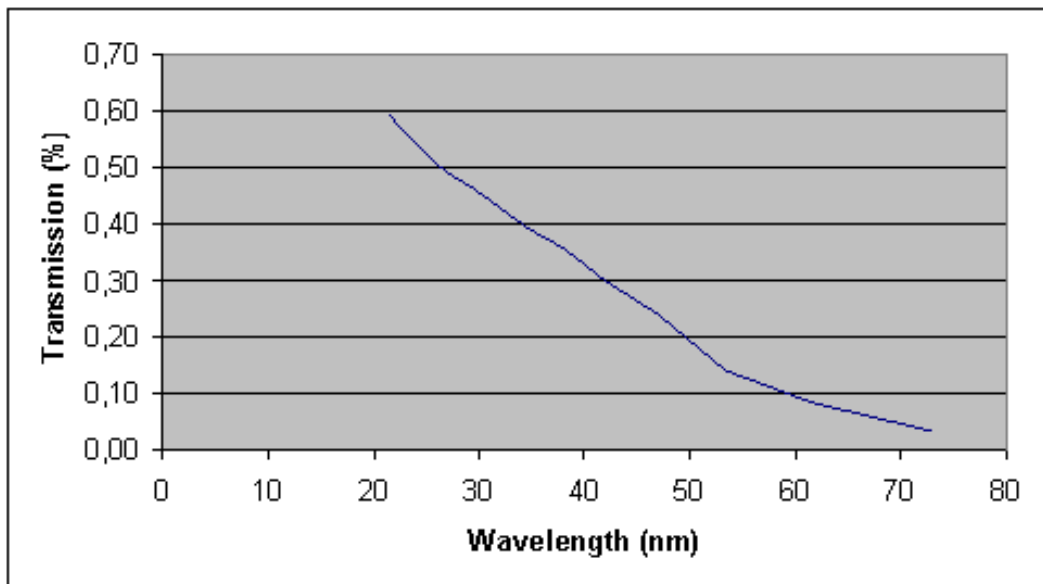Figure 3.10: Harmonic spectrum with and without filter. Backing pressure 1 atm.

Figure 3.11: Simulated transmission of aluminium filter with oxide layer.

Chapter 4

Experimental Method and Results

This chapter will present the three holographic experiments that have been carried out. Each with a more complicated setup and more taxing conditions that the previous. The first experiment that is presented is carried out with a continous He-Ne laser. The second is with the infrared laser pulses from the terawatt laser. The pulses will be used to generate the harmonics which the third experiment is carried out with. The idea has been to gradually increase the level of complexity in order to foresee and handle pending problems. Further the various setups have afforded the opportunity to test the reconstruction program on several different conditions allowing for a greater knowledge of its pros and cons. However, first a short section will present some preparatory calculations that have been made in order to determine the limitations the experiments are subject to.

4.1   Preparatory Calculations

Before undertaking any kind of experiment it is vital to make sure that it takes place within the boundaries of what it actually physically possible. Two constraints have been defined as vital - that at least the radius of one diffraction ring should fit the recording chip and how much of the beam the object blocks. The calculations have been performed for the final experiment since that is the goal of the thesis. The first constraint can be found through the formula for the resolution limit:

$$a \leq \frac{1,22\lambda}{2sin\theta} \rightarrow L \leq a \cdot \frac{D}{1,22\lambda} \tag{4.1}$$

where the parametres are defined according to figure 4.1.

The equation can be rewritten as above since the angle is small. The size of the objects can be assumed to be approximately 50 μm and the wavelength is approximately 40 nm, since we can assume that it will be around the 20th harmonic. The width of the CCD chip $D = 8,8$ mm. These settings lead to $L \leq 9$ m. However since it is the radius of the diffraction ring that is of concern the experimental boundary will be $L \leq 18$m.

To figure out how large the object can be, the Fraunhofer condition, equation 2.6 is used. Assuming the distance between the focus of the beam and the object to be 1 m
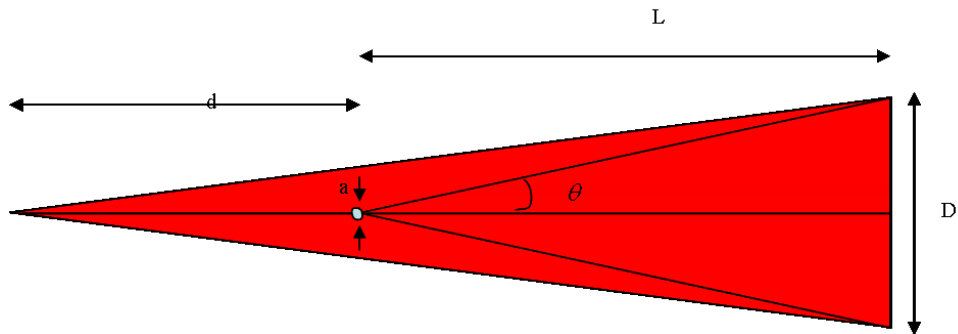
Figure 4.1: Resolution parameters.

and the same wavelength as above it turns out that $a \ll 200\ \mu$m. Since the objects in the experiments are hairs which can be expected to have a thickness of approximately $50\ \mu$m, the final experiment is on the limit. Since other similar experiments have taken this condition as more of a guidance than an absolute rule, the experiments will be carried out with hairs as planned.

4.2 Experiment with a HeNe Laser

4.2.1 Setup

The setup for this experiment is very simple and is illustrated in figure 4.2. The laser beam is directed through a spatial filter. The spatial filter is simply a lens with a pinhole in the focal plane. It creates a divergent beam. The object is placed in the beam after the spatial filter at approximately one third of the distance between the spatial filter and a CCD creating a geometrical magnification of a factor of roughly 3. The CCD camera which is connected to a computer records the interference pattern. To record a reference picture the object is simply removed from the setup and another picture is taken. Two polarisers are part of the setup although not included in figure 4.2. They are there so that the intensity of the beam can be varied in order to record a maximum intensity with the CCD camera which is in the region of, yet below, its saturation intensity. The spatial filter also plays a role in reducing the intensity since it widens the radiation cone of the beam. Finally, the shutter speed of the CCD camera can be varied too.

4.2.2 Results

The holographic experiment was carried out with a couple of hairs. The resolution of the CCD chip is $6\ \mu$m. In figure 4.3 the hologram, the reference, and the hologram subtracted from the reference are shown. Reconstructing with the hologram alone would work just as well. However, subtracting does get rid of some spots that can be seen in the reference beam. Also fringes can be seen in the images. In an ideal case they would disappear with the subtraction. However, even the slightest instability would cause the fringes to prevail as they have done in figure 4.3 C. The fringes are carried into the reconstruction as can be seen in figures 4.4 and 4.5, but do not affect the visibility of the reconstructed object in any greater fashion.
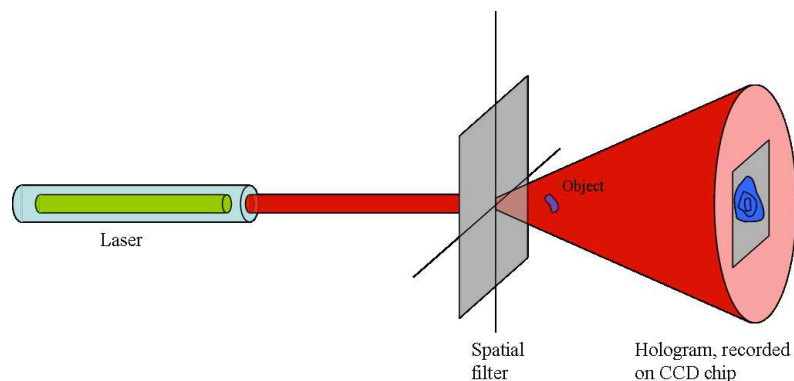
Figure 4.2: The setup for digital in-line holography with the HeNe-laser.

In figure 4.4 the object has been reconstructed at three different distances from the CCD camera. It can clearly be seen that the reconstruction at 10 cm provides the image closest to the focal plane. The axes are numbered in microns. In the other reconstructions only one of the hairs is clearly visible and the other one is either blurred or not very clearly defined. Around the thicker of the two hairs the twin image can also be seen to vary in size and definition as the distance varies.

Having found an approximate distance to recreate the objects in, it is easy to close in on the focus of the image and improve the recreation. The optimal distances were found to be 10 cm and 9.6 cm as shown in figure 4.5. By determining the coordinates with the aid of MatLab the width of the hairs was found through applying the Pythagorean Theorem. The results, 0.04 mm and 0.1 mm will have to be divided by the geometric magnification factor which is $252/(252 - 100) = 1.7$. This leads to a thickness of the hairs of 24μm and 59μm respectively. This corresponds well to the thickness hair has in general although the thinner hair is slightly too thin. However it could very well be the end of a hair, or perhaps even a split end.

4.3 The Experiment with The Pulsed Laser

4.3.1 Setup

The setup of this experiment is only slightly more complicated than that of the previous one. The laser beam being used is the terawatt laser at the Lund High-Power Laser Facility. The system delivers ten pulses per second at 800 nm which are approximately 35 fs each. The beam diameter is approximately 4 cm $(1/e^2)$ and the pulse energy is roughly 100 mJ. This boils down to three specific problems for this particular experiment. The intensity must be reduced so that the CCD chip does not read maximum intensity at every point. A CCD camera that functions in the infrared is needed, and finally it must also have a possible shutter time of, at the most, 0.1 s.

Such a CCD camera was found, the Star CCD. The camera is connected to a monitor and is possible to remote control by a computer. A short instruction how to operate the camera and its software is found in appendix C. For now the necessary information about the camera is that it detects light in the IR-region and that the resolution of the CCD chip is 23 μm.
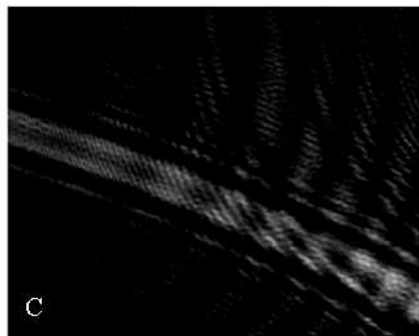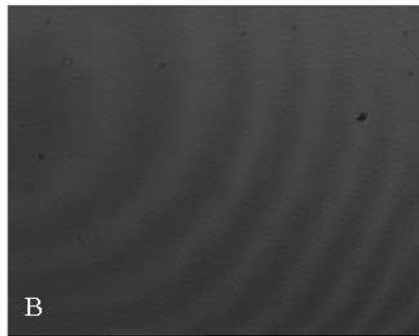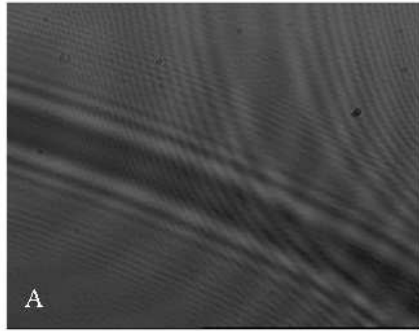
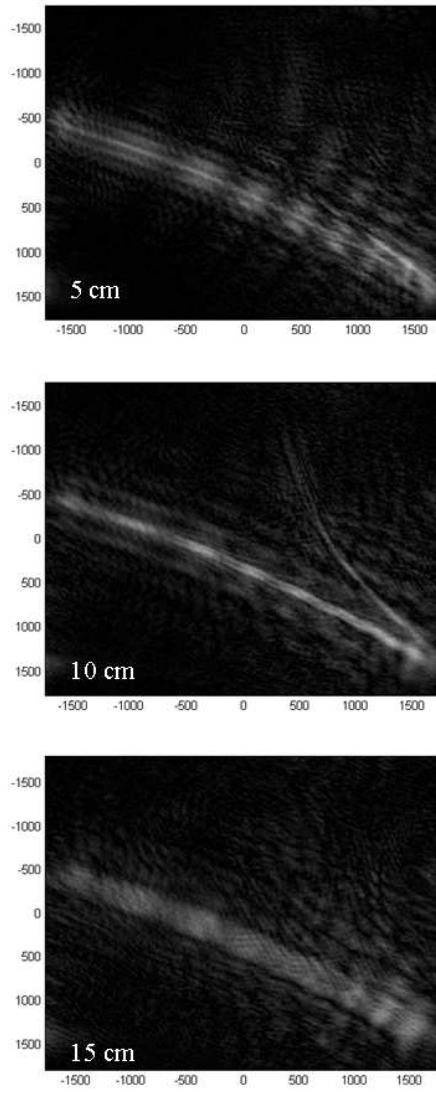Figure 4.3: The pictures taken by the CCD camera

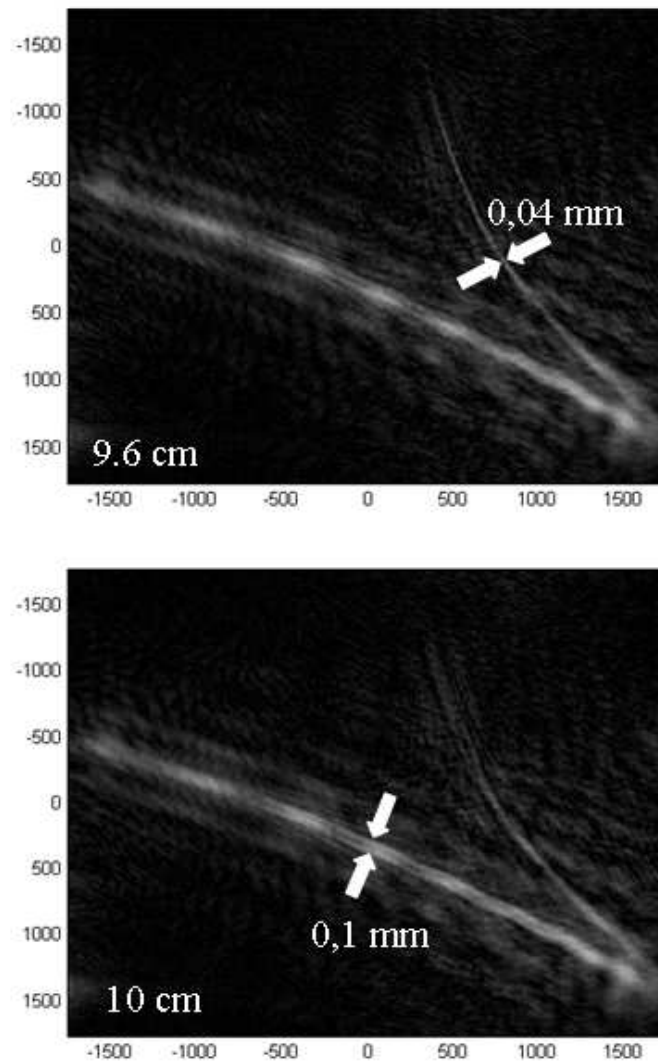Figure 4.4: Reconstructed images at three different distances.

Figure 4.5: Reconstructed images at optimal distances with the size of the objects measured.

The setup is illustrated in figure 4.6. Omitted from the illustration are the windows and polarisers used to reduce the intensity of the beam. The focal length of the lens used is -176 mm, which suffices for the radiation cone to well and truly cover the CCD chip. The object is placed 5 cm from the lens.
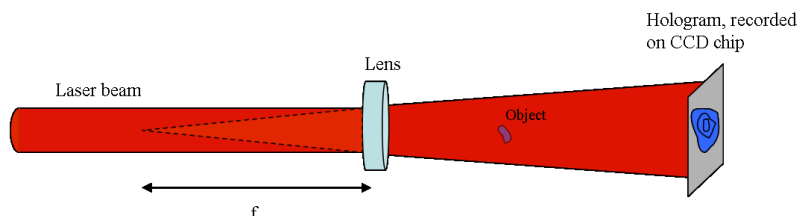

Figure 4.6: The setup for digital in-line holography with the pulsed laser.

4.3.2 Results

The results of this experiment will be presented in the same way as the results of the experiment with the HeNe-laser. First, images of the recorded hologram will be presented. They will be followed by images reconstructed at various distances from the CCD camera. The reconstruction is done with the hologram alone this time. The reason for that is that the recorded reference beam and the hologram do not match each other well enough. This leads to severe problems in the reconstruction process. Effectively the framing effect, discussed in the section on the simulations, takes over. The way around this is to make sure the borders of the picture are close to zero or far away from the region of interest. However any large difference in 'intensity' along a straight line seems to cause problems and should consequently be removed.

The problems have been solved by inserting a frame around the hologram which has an intensity equalling the average intensity of the borders of the hologram. In addition the hologram has ben cut around the left edge to remove the completely black area there. Also the image has been cut along the bottom to remove the black area and the white streak. These adjustments can be seen in the bottom image in figure 4.7. The top image is the hologram prior to the modifications.

In figure 4.8 the hairs have been reconstructed at the distances of 10, 20, and 30 centimeters. Clearly the reconstruction at 20 cm provides the best image since the hairs are wider in the other images. Reconstructing images at several different planes is the easiest way to determine where the focus may be, since the image will be wider both before and after the focal plane. As it was not possible to subtract the hologram from the reference beam in this experiment some spots are carried over into the reconstruction. They become less visible as the distance is increased – a sign that they are due to some dirt on the CCD chip or thereabouts.

Figure 4.9 shows the reconstructed image in the focal plane 18 cm from the CCD, which is the plane that provides the best reconstruction image. Through measurements in the image the hairs are found to be 0.1 mm thick. The geometric magnification factor is $(180 + 174 + 50)/(174 + 50) = 1.8$ leading to a thickness of 56μm of the hairs. However since the resolution is as low as 23 μm it is only approximately 13μm after the magnification which is a pretty crude approximation. In any case, the results are in the right region. One interesting effect which can be seen in the image is the
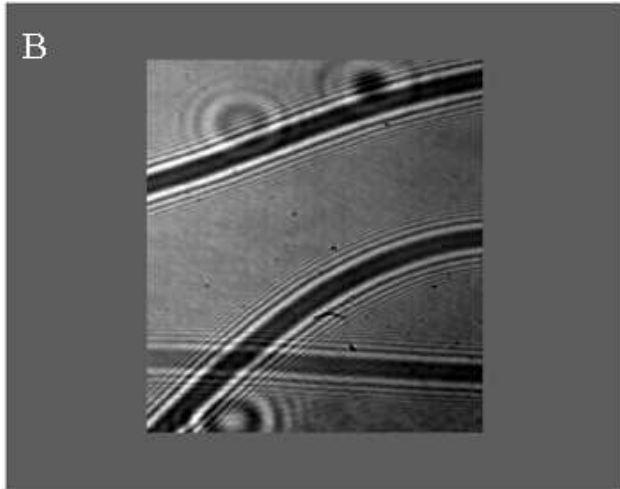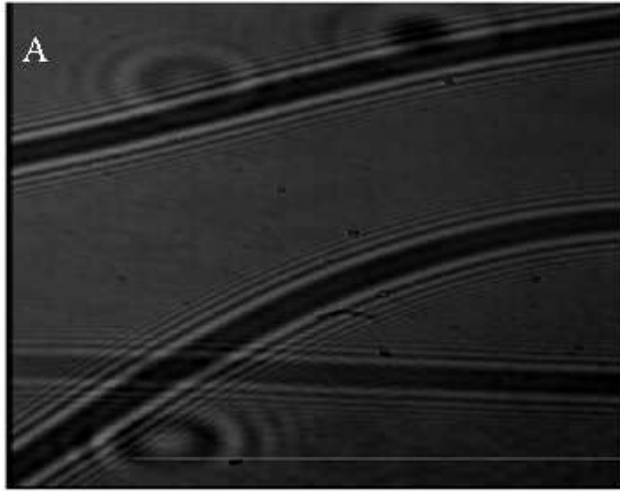
Figure 4.7: Top: Hologram before modification. Bottom: Modified hologram. The size and the scaling is indifferent in these images, that will be paid attention to in the reconstructions.
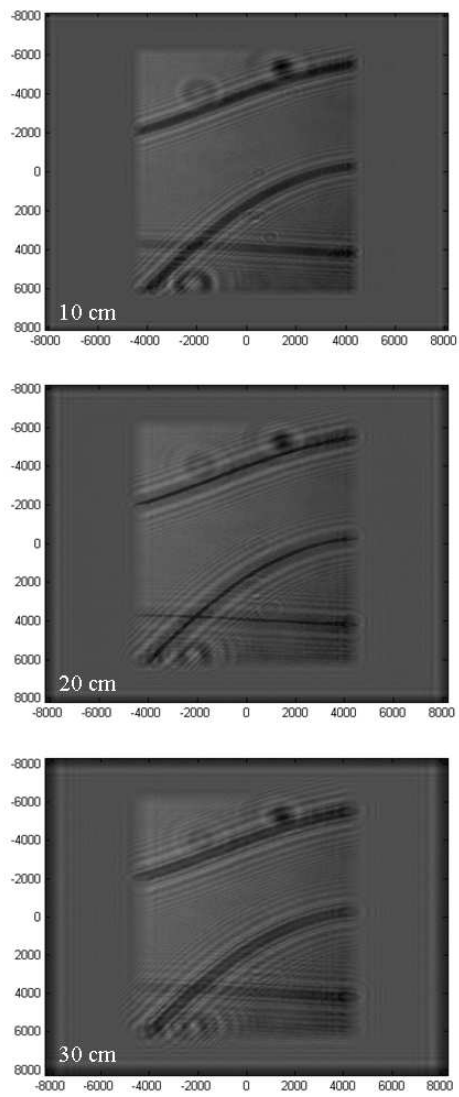
Figure 4.8: Reconstructed images at three different distances.

effect of the hairs at the edges of the hologram. This is the effect that previously has been labelled the framing effect. It is evident that the difference in intensity has a large impact on 'the progagation of the frames'.
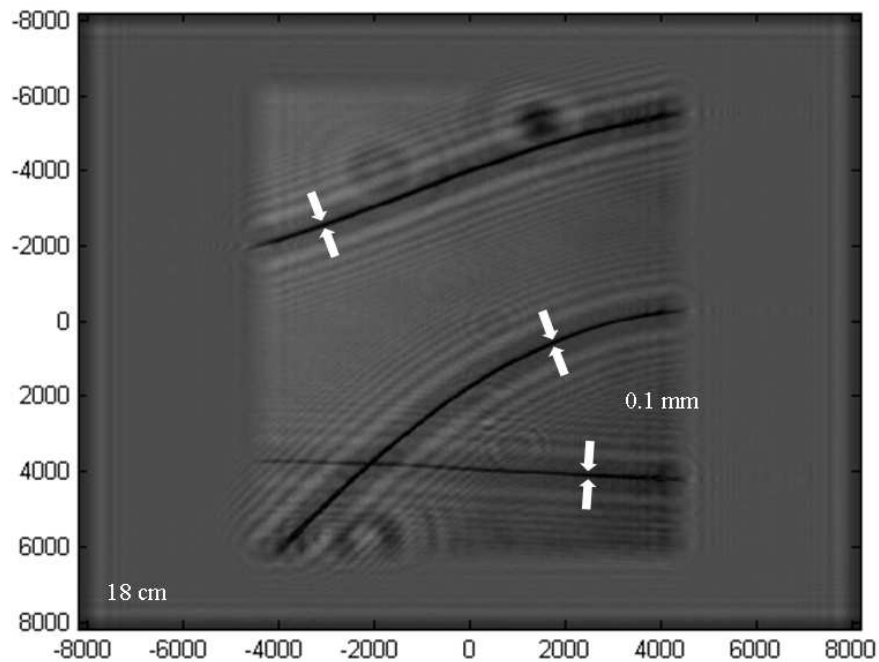
Figure 4.9: Reconstructed image at 18 cm.

4.4   Holography with Harmonics

4.4.1   Setup

Three main problems complicate the setting up of this experiment. First the experiment needs to be carried out under vacuum. This is due to the harmonic generation process. Vacuum is also needed for operating the MCP (Micro Channel Plate) The MCP adjoined to a phosphor screen is necessary for imaging in the generated wavelengths and for it to be operable the pressure needs be below 10^{-5} mBar, at the most. The second difficulty is the necessity to image the picture on the phosphor screen onto the CCD. In order to get a clear picture of the MCP screen of the right size unconventional measures had to be taken. The third problem is inserting the object into the beam path. All three problems will be treated in more detail below. Figure 4.10 is a schematic illustration of the setup.
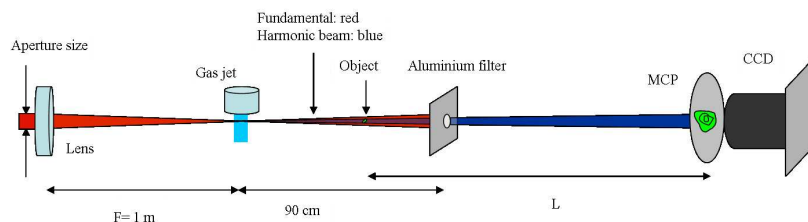
Figure 4.10: Setup for holography with high harmonics.

The MCP

An MCP basically functions as a photo multiplicator. Electrons are ionised through the photoelectric effect when they collide with a metal plate. These electrons are accelerated in an electric field and collide with another metal plate where several electrons are ionised foreach colliding electron - these electrons finally collide with a fluorescent screen. Since the initial metal plate is divided into many small parts the process of accelerating the electrons takes place separately for each small part leading to an image on the fluorescent screen; an image which is proportional in intensity to the initial distribution of electrons colliding with the MCP.

This requires a high voltage. The voltage used in the experiments carried out here was 3500 V on the positive side and -1500 V on the negative side. Since this is a large difference in potential with the cathode and anode fairly close to each other, the voltages are applied incrementally according to a manual. Although time consuming, it is a necessary process.

The CCD and Focusing

The CCD camera comes with a 50 mm $\frac{f}{1.8}$ lens. This is used to take pictures of the display of the MCP. However, in order to optimise the size of the picture, the lens of the camera is not mounted to the camera in the regular fashion. It is fastened approximately 1 cm in front of its normal mount. This way the picture of the MCP projected onto the CCD-chip is of the size that leads to an optimal resolution. This was ascertained through measuring the size of the image on the MCP. That size multiplied by the factor of the CCD-screen resolution divided by the MCP resolution leads to the minimum size of the image on the CCD-screen which entails no loss of information. Following the setting up of the equipment in this fashion it is a mere formality to change the settings of the lens in order to obtain the clearest image.

Placing The Object in The Beam Path

As no useful equipment was available, a device had to be created in order to insert the object into the beam path. The simplest possible device was created. A square with sides of approximately 7 cm was cut out of copper foil. In the middle of this the inner diameter of the vacuum tubes was marked (4 cm). The foil was then cut so that the remainder resembled a square cross with a 4 cm diameter circle superimposed. The ends of the cross were then bent alternatively forward and backwards providing a simple means to fasten the device to the inside of the tube. Fastening the object to the device was simply done with Scotch tape. This simple construction enabled moving

the object to various places along the setup affording the opportunity to perform the experiment at different lengths between the object and the MCP. In the setup presented here the object was placed 45 cm from the focus of the beam.

4.4.2 Optimisation

Before proceeding with the holography it is in order to present the pictures taken to optimise the settings with the MCP. Since the MCP provides a completely different way of visualising the spectrum to the spectrometer this is of the greatest necessity. In the following figures the aperture and the distance between the lens and the gas jet have been varied respectively, while the backing pressure has been kept at 0.8 atmospheres. In figure 4.11 the aperture has been varied in 2 mm increments from 6 mm to 12 mm. The most useful image is obtained with the aperture at 10 mm, although the image with the aperture at 12 mm is almost as good. What constitutes a good image is being able to see an as clear image as possible of the harmonic beam that passes the aluminium filter. An intresting detail in these images is that a small crease can be seen in the top left of the images. This is a crease in the aluminium filter that is used.

Assuming the 10 mm aperture to be the optimal aperture the distance between the gas jet and the lens is varied in figure 4.11. The distance is varied in 10 mm increments around the approximate focal distance of 1 m. The notations in the figures are on a different scale and in millimeters as explained in the subsection named *Varying the Focal Point*. Clearly the best images are the ones taken at 360 mm and 370 mm in which the full aluminium filter can be seen in relatively good detail. Although the object of the setup by no means is to view the aluminium filter, a good image of it is a welcome indication. Also, by imaging as much as possible of it, more information will be there for the processing when the actual holographic reconstruction is made. The setting at 360 mm was chosen to be the best image.

4.4.3 Results

After deciding the optimal setting the object is inserted into the beam path. As in previous experiments the object consists of a couple of hairs. After inserting the object the focusing is tuned in order to obtain the clearest possible image. Although the previous images had certain structure, the additional structure provided to the image from the object, enables further enhancement of the focusing. Figure 4.13 is the best imaged obtained, thus being the image which will be used for holographic reconstruction. This image was obtained, as can be concluded from the previous section, with an aperture of 10 mm, a distance between the lens and the gas jet at the setting of 360 mm, and a backing pressure of 0.8 atmospheres. The distance between the object and the MCP, indicated by L in figure 4.13 was measured and found to be 1.80 meters. Subtracting the best picture from a background picture created an inverted image of which the relevant parts were cut out. As can been seen in figure 4.14 the noise is on a relatively low level. This inverted image is the image used throughout the reconstruction process. In fact the reconstruction process was carried out with the unprocessed best image too. The same results were arrived at, but since the inverted images were deemed to better from an illustrative point of view they are the ones included here. All reconstructinos were done using the 21:st harmonic. One harmonic was chosen since, according to the simulation, it does not seem to matter whether one or several harmonics are chosen. The choice of harmonic may as well have been the 19:th since the choice was made on the basis of the transmitted intensities displayed in figure 3.10.
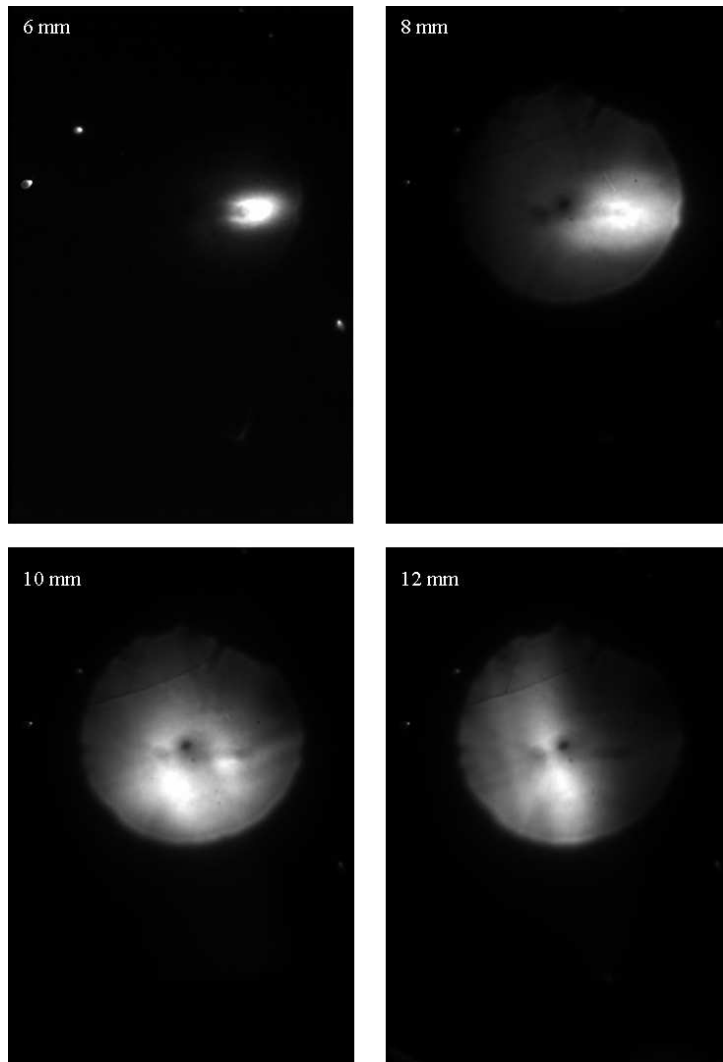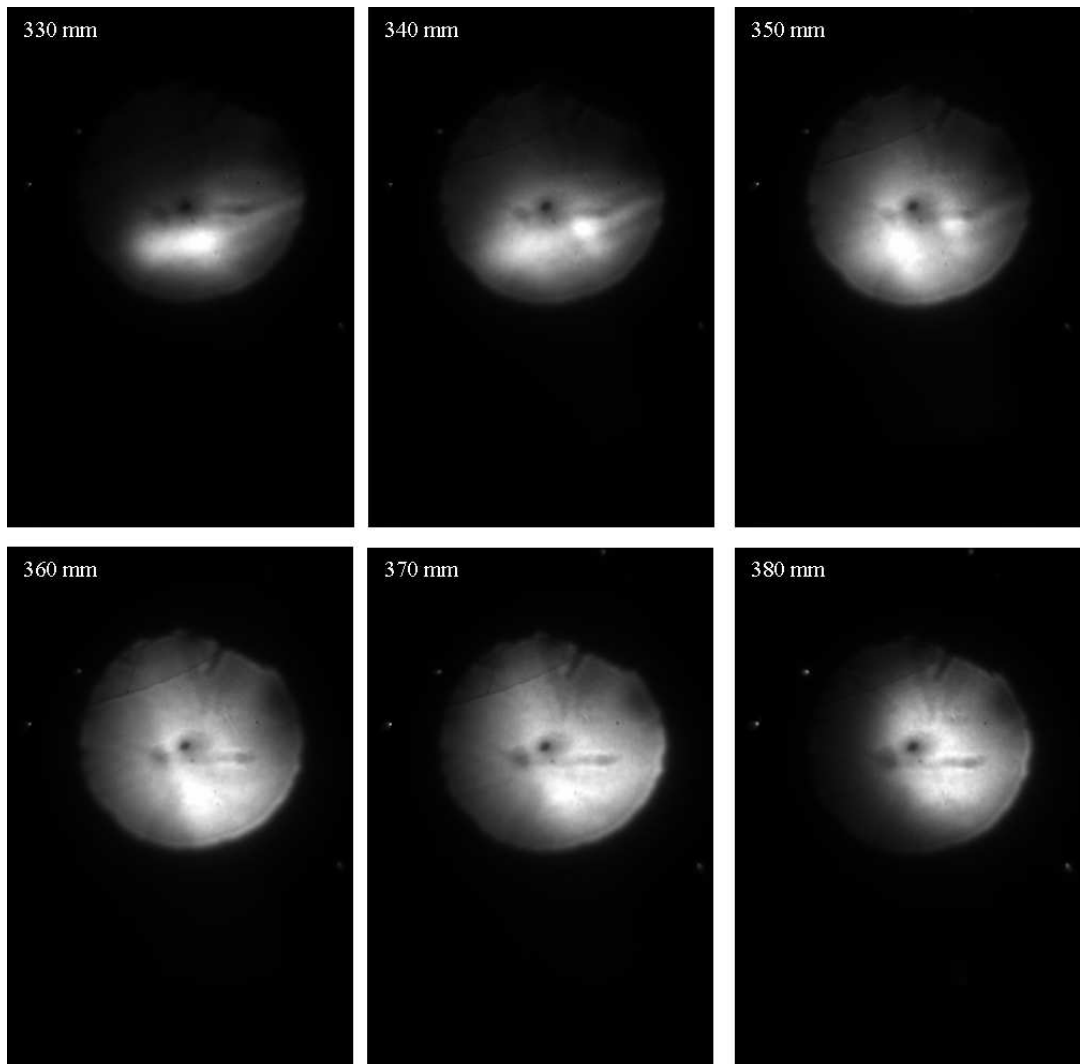
Figure 4.11: Varying the aperture.

Figure 4.12: Varying the distance between the object and the lens.
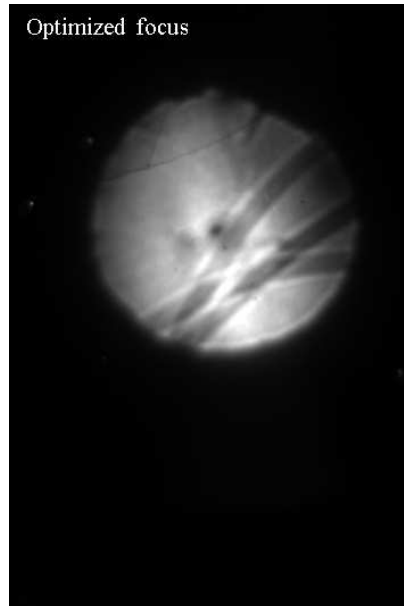
Figure 4.13: The best picture.
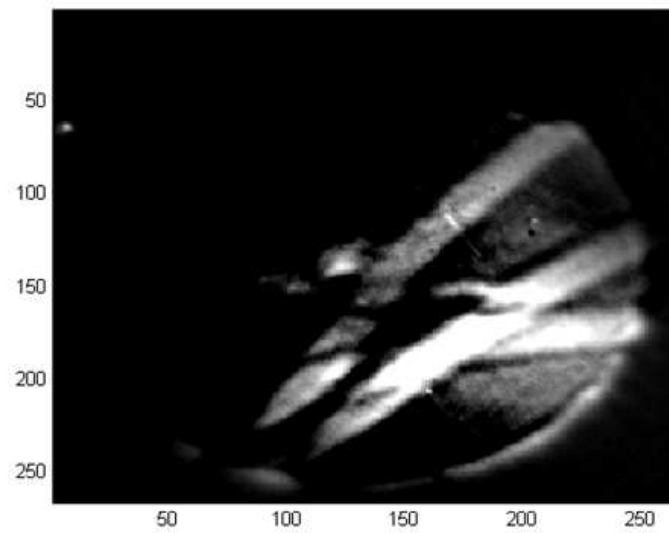
Figure 4.14: The best picture subtracted from the background.

Figure 4.15 displays the reconstructed images at 120, 180, 240, and 300 centimetres. The images are pretty similar but the ones at 180 and 240 centimetres are the best. This is determined through observing how the top hair is the thinnest at this distance. In order to further close in at which distance the image can be considered to be the best a recreation was made at 20 cm intervals in the range from 120 cm to 300 cm. In figure 4.16 the three best recreations are presented, the ones at 180, 200, and 220 cm. There is not much in it, but if once again the thickness of the hairs is closely examined, the image at 180 cm is the best. However the two lower hairs contrast more against the background in the two other images. Unfortunately I have not been able to figure out what causes this, but the occurrence seems to become more marked as the reconstruction distance increases. This can be seen in figure 4.15 in the reconstruction made at 300 cm.
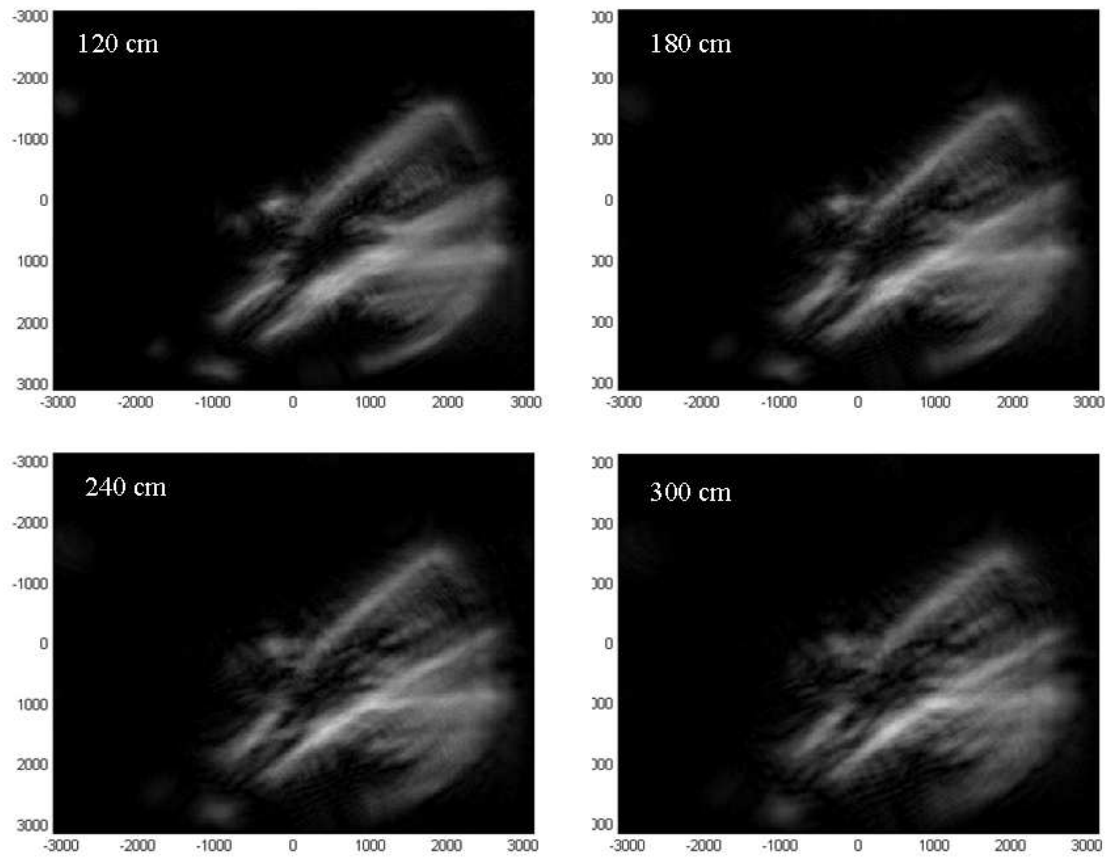
Figure 4.15: Four different recreation distances.

In the reconstructions carried out, the images have not become at all as clear as the ones in the previous two experiments. This is unfortunate, but not wholly unexpected. After all the simulation with several harmonics indicated that the images would become somewhat blurred. The blurriness is also partly an explanation to why the recreation
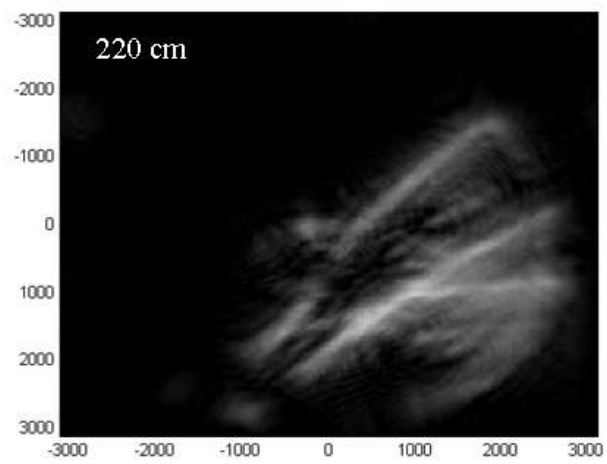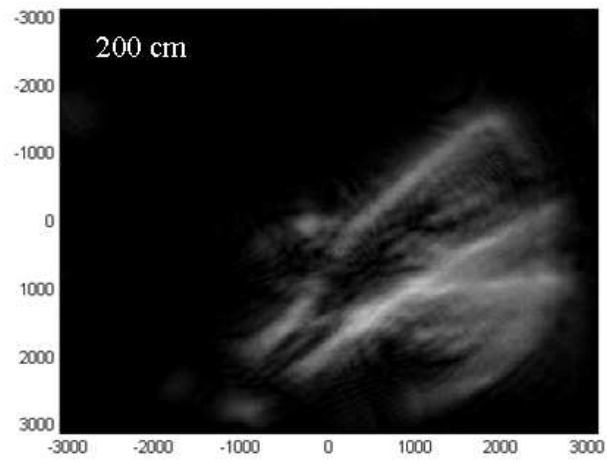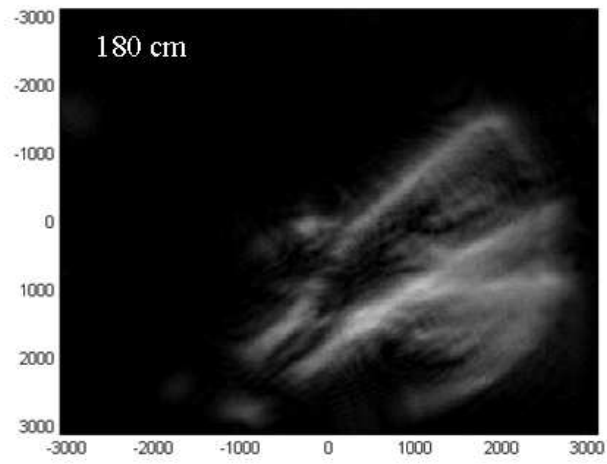
Figure 4.16: Three recreations.

intervals aren't smaller. To find the focus there after all has to be a clear focal plane. Partly this can also be explained by the beam being so close to parallel. Apart from the wavelength the width of the beam at the recording device has determined the distance to the object. A comparison with the other two experiments leads to this assumption. Trials were carried out with a pinhole to create a more divergent beam but they led nowhere.

Despite the blurriness of the reconstructed image the width of the hairs was measured. As displayed in figure 4.17 it was found to be 0.12 mm. This is slightly wider than previously. However this is most probably due to a larger magnification factor which is $(180 + 45)/45 = 5$. Taking this into consideration the thickness of the hairs is 24μm and the resolution 5μm. The thickness is slightly lower than expected, however the blurriness of the image makes it hard to determine the exact thickness of the hairs.
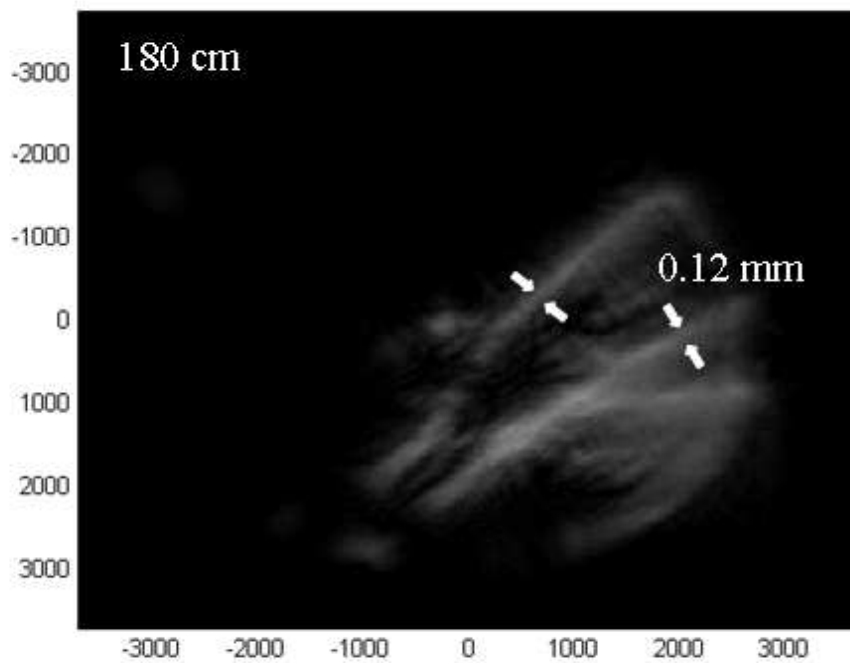
Figure 4.17: The chosen recreation with measurements in the figure.

Chapter 5

Concluding remarks

5.1 Summary and Conclusions

A reconstruction program for digital in-line holography has been created, tested and implemented. With the aid of this program in-line holography was successfully carried out with high harmonics, as was the goal of this thesis. Although there are many improvements that can - and should - be done, this is a first step towards successfully performing holography with extreme ultraviolet radiation.

The results from the simulation concur satisfactorily with the results from the three experiments where in-line holography was done with hairs. The reconstructive process seems to suffer from the presence of several wavelengths. Also it is clear from the experiment with the pulsed laser that the reconstruction algorithm is very sensitive to the boundary conditions of the holographic image. The program recreates images of the objects with the best recreation at the correct distance from the recording device. Further, the size of the objects in the recreated images are of the right size.

The fist experiment was carried out with a HeNe laser and the hairs were found to be 24μm and 59μm thick. The second experiment was carried out with a pulsed Ti:sapphire laser and the thickness of the hairs was found to be 56μm. The final experiment was carried out with high harmonics and the hairs measured 24μm across. The images were slightly blurred in the final experiment which was foreseen by the simulation.

Since the project has been in the outskirts of what the group has been working on, the work has been carried out independently of the group. This has both advantages and drawbacks. The advantages are on an individual plane in the form of an increased control of the project and the increased confidence in one's own ability to achieve set goals. The drawbacks are due to the lack of someone with a complete insight into issues working by one's side. There is nothing like continual fruitful cooperation for overcoming difficulties, improving ideas and achieving results. However the overwhelming helpfulness and expertise I have encountered and had the opportunity to draw on, have doubtlessly reduced the drawbacks to a minimum.

Performing holography with high harmonics brings together two different areas of expertise, holography and high harmonic generation. Since this is new to the department the goal of the thesis has been the proof of the principle rather than any kind of optimisation, and it is in this light the results should be viewed.

5.2 The next step

Even though the goal of the thesis has been reached, there is of course plenty of room for improvement. In this section I intend to discuss some areas of the project, which I deem the most readily improvable. The discussion is divided into two parts, *Improving the Reconstruction Algorithm* and *Experimental Improvements*.

5.2.1 Improving the Reconstruction Algorithm

There are two main areas in which an improvement of the reconstruction algorithm would be useful. The reconstruction algorithm treats the light that creates the hologram as if it were a plane wave. This has proven to be a pretty good approximation, but it would have been better if the algorithm could be implemented, taking the spherical nature of the wave fronts into consideration. This modification would enable in-line holography to be used even more as a means of magnification. This is done through experimentally creating a wider radiation cone, thus making it possible to move the light source, object and recording device much closer to each other. This would however entail processing the image information differently in the reconstruction program. In this case the pixels would have to be treated as area elements on the face of a sphere.

The other improvement, which would improve the reconstruction algorithm, would be to implement the iterative process of reconstructing described in section 2.4. This was attempted without any success. However, despite this, I am adamant that it should not be too hard to succeed with the implementation.

5.2.2 Experimental Improvements

The main improvements that can be made here come through clearly in the discussion of the results. First of all it seems important to single out one harmonic. This is possible, though expensive. Furthermore, especially designed multilayer mirrors mirrors that are capable of doing this, function at normal incidence. Therefore installing such a mirror in the setup would entail rebuilding the whole setup. Another improvement that is vital is the resolution. Holography with harmonics naturally needs to be carried out with fairly small objects. Without equipment with high enough resolution to accommodate for this, truly satisfactory results can never be obtained. There is however, perhaps, a way around this problem. By blowing up the beam in the fashion briefly described in the previous section, the resolution will not be as vital. However this would entail rebuilding the setup and the programming efforts mentioned above. Also, I believe it would require a higher intensity of the harmonic beam than the system delivers at present.

Chapter 6

Acknowledgements

It is hard to know where to begin considering the overwhelming helpfulness I have encountered from everyone at the department whom I have had the fortune to be in touch with. However a few people have stood out, playing key roles, enabling the successful completion of this thesis. First and foremost my supervisor Anne L'Huillier has, through numerous discussions, been the guiding light of my exploits within physics and generously shared her superior knowledge of experimental design. In Sven-Göran Pettersson, who has been immensely helpful with his vast expertise of holography, I had had the fortune to find a second supervisor. Claes-Göran Wahlström has been of great help, especially when it comes to solving experimental problems. Several times when I have begun to despair he has solved, to me, seemingly insurmountable problems. Finally I would like to thank Thomas Lennartsson who has come to my aid the innumerable times I have not been on equal terms with my computer and kept my spirits up with many revitalising discussions in the realms of political philosophy.

Bibliography

[1] R.A. Bartels, A. Paul, H. Green, H.C. Kapteyn, M.M. Murnane, S. Backus, I.P. Christov, Y. Liu, D. Attwood, C. Jacobsen. *Generation of Spatially Coherent Light at Extreme Ultraviolet Wavelengths.* Science, Vol.297 (2002)

[2] D.G. Lee, J.J.Park, J.H. Sung, H. Nam. *Wave-front phase measurements of high-order harmonic beams by use of point-diffraction interferometry.* Optical Letters, Vol.28, No.6 (2003)

[3] Dennis Gabor. *Nobel Lecture - Holography, 1948-1971* (1971)

[4] Sven-Göran Pettersson *Holografi.*Lund. (1997)

[5] Ulf Schnars, Werner P.O. Jüptner. *Digital Recording and numerical reconstruction of holograms.* Measurement Science and Technology Vol.13 (2002)

[6] Ulf Schnars, Werner P.O. Jüptner. *Digital recording and reconstruction of holograms in hologran interferometry and shearography.* Applied Optics, Vol.33 No.20 (1994)

[7] M. Gustafsson, M. Sebesta, B. Bengtsson, S.G. Pettersson, P. Egelberg, T. Lenart. *High-resolution digital transmission microscopy – a Fourier holography approach.* Optics and Lasers in Engineering, Vol.41 (2004)

[8] H.J. Kreuzer, R.A. Pawlitzek *Digital in-line holography* Europhysics News, Vol.34 No.2 (2003)

[9] W. Xu, M.H. Jericho, I.A. Meinertzhagen, H.J. Kreuzer, *Digital in-line holography for bioloical applications.* PNAS, Vol.98 No.20 (2001)

[10] G. Koren, D. Joyeux, F. Polack. *Twin-image elimination in in.line holography of finite-support complex objects.* Optics Letters, Vol.16 No.24 (1991)

[11] X.M.H. Huang, J.M. Zuo, J.C.H. Spence. *Wavefront reconstruction for in-line holograms formed by pure amplitude objects.* Aplied Surface Science Vol.148 (1999)

[12] I. Yamaguchi, J. KAto, S. Ohta, J.Mizuno. *Image formation in phase shifting digital holography and applications tp micoscopy.* Applied Optics, Vol.40 No.34 (2001)

[13] Lena Roos.*Optimisation and Application of Intense High-Order Harmonic Pulses.* PhD Thesis, Lund Institute of Technology, LRAP-276 (2001)

[14] Johan Norin. *Characterisation and Application of Ultrashort Extreme Ultraviolet Pulses.* PhD Thesis, Lund Institute of Technology, LRAP-289 (2002)

[15] Stefan Hässler, Marko Swoboda. *Optimization and Application of High-order Harmonics of an Ultrashort Terawatt Laser.* Lund Institute of Technology, LRAP-324 (2004)

Appendix A

The Simulation Program

```
clear all;
close all;

%Inparameters
N=256; %Matrix size
a_obj=10; %sample interval in plane Obj
pi=3.14159;
sigma=15; %the radius of the Gauss function at 1/e
L1=4*10^6; %distance to far field plane in microns
L=.4*10^6;    %distance between hologram and object
Lref=L+0.2*10^6;    %Distance between refence point and object
L2=L1-L;
lambda_laser=0.8; %wavelength in microns
min_harmonic=23;
max_harmonic=23;
lambda_sample=lambda_laser/max_harmonic;
a_far=lambda_sample*L1/(N*a_obj); %sample interval in plane Far
a_hol=L2/L1*a_obj; %sample interval in plane Hol


%Planes
%plane Obj
xvec=-N/2*a_obj:a_obj:(N/2-1)*a_obj; %element N/2+1 has coord 0
yvec=xvec;
[xmat,ymat]=meshgrid(xvec,yvec); %the coord matrices
objradius=sqrt(xmat.^2+ymat.^2);

%plane Hol
hxvec=-N/2*a_hol:a_hol:(N/2-1)*a_hol; %element N/2+1 has coord 0
hyvec=hxvec;
[hxmat,hymat]=meshgrid(hxvec,hyvec); %the coord matrices
holradius=sqrt(hxmat.^2+hymat.^2);

%Plane Far
fxvec=-N/2*a_far:a_far:(N/2-1)*a_far; %element N/2+1 has coord 0
```

```
fyvec=fxvec;
[fxmat,fymat]=meshgrid(fxvec,fyvec); %the coord matrices
farradius=sqrt(fxmat.^2+fymat.^2);

%Plane of Reference
a_ref=a_far*L1/Lref;
refxvec=-N/2*a_ref:a_ref:(N/2-1)*a_ref; %element N/2+1 has coord 0
refyvec=refxvec;
[refxmat,refymat]=meshgrid(refxvec,refyvec); %the coord matrices
refradius=sqrt(refxmat.^2+refymat.^2);

%The picture
impobject=imread('teckning.bmp');
object=impobject(1:N,1:N);

%Gaussian beam
gaussfunc=exp(-(objradius.^2)/sigma^2);
%Gaussian beam after object (still plane Obj)
E_obj=gaussfunc.*object;

%Visualisation:
%Intensity of gaussian beam after object (still plane Obj)
I_obj=abs(E_obj).^2;
figure(1)
colormap(gray)
image(xvec,yvec,I_obj*64)

I_hol=zeros(N);
I_obj_rev=zeros(N);
count=0;
while min_harmonic<=max_harmonic
    k=2*pi*min_harmonic/lambda_laser; %wave number

    %The hologram
    G=L2/L1.*exp(i*k*(L1-L2)).*exp(i*k/2*farradius.^2*(1/L1-1/L2));
    Obj_plane=E_obj.*exp(i*k*objradius.^2/(2*L1));
    E_hol=exp(-i*k.*holradius.^2/(2*L2)).*ifft2c(G.*fft2c(Obj_plane));

    I_hol=abs(E_hol).^2+I_hol;
    min_harmonic=min_harmonic+2;
    count=count+2;
end
min_harmonic=min_harmonic-count;

%Visualisation:
%Intensity of beam at hologram
figure(2)
colormap(gray)
image(hxvec,hyvec,I_hol*64/(count/2))
j=3;
```

```matlab
while min_harmonic<=max_harmonic
    k=2*pi*min_harmonic/lambda_laser; %wave number

    %The object revisited
    F=L1/L2.*exp(i*k*(L2-L1)).*exp(i*k/2*farradius.^2*(1/L2-1/L1));
    Hol_plane=sqrt(I_hol)./(count/2).*exp(i*k*holradius.^2/(2*L2));
    E_obj_revisited=exp(-i*k.*objradius.^2/(2*L1))
    .*ifft2c(F.*fft2c(Hol_plane));

    I_obj_rev=abs(E_obj_revisited).^2;
    %Intensity of beam at the "revisited" object

    figure(j)
    colormap(gray)
    image(xvec,yvec,I_obj_rev*196)
    title(['Reconstructed with harmonic ',num2str(min_harmonic),'.'])
    min_harmonic=min_harmonic+2;
    j=j+1;

end
```

Appendix B

The Holographic Reconstruction Program

```
clear all;
close all;

%Inparameters
N=266; %Matrix size
a_hol=23; %sample interval in plane Obj
pi=3.14159;
sigma=1000; %the radius of the Gauss function at 1/e
L1=100*10^6; %distance to far field plane in microns
min_L=1.8*10^6; %distance between hologram and object
step=2*10^5; %length of steps
max_L=min_L+step*1;
Lref=min_L+0.9*10^6;      %distance between refence point and object

lambda_laser=0.8; %wavelength in microns
min_harmonic=21;
max_harmonic=21;
lambda_sample=lambda_laser/max_harmonic;

%The imported hologram
impobject=imread('05060700.bmp');
[m,n]=size(impobject);
impobject=impobject(75:340,75:340);
[m,n]=size(impobject);

%The imported reference
impobject2=imread('05060707.bmp');
[m2,n2]=size(impobject2);
impobject2=impobject2(75:340,75:340);
[m2,n2]=size(impobject2);

%Creating the processed image
```

```
impobject=(impobject2-impobject);
I_hol=double(impobject);


%Visualisation

figure(1)
colormap(gray)
image(imread('05060700.bmp')/4)
title('Object picture')

figure(2)
colormap(gray)
image(imread('05060707.bmp')/4)
title('Reference')

figure(3)
colormap(gray)
image(impobject)
title('Object minus reference ')

I_obj_rev=zeros(N);
count=0;
j=4;

while min_L<=max_L

    k=2*pi*min_harmonic/lambda_laser; %wave number
    L2=L1-min_L;

    %Planes
    %plane Obj
    a_obj=L1/L2*a_hol; %sample interval in plane obj
    xvec=-N/2*a_obj:a_obj:(N/2-1)*a_obj; %element N/2+1 has coord 0
    yvec=xvec;
    [xmat,ymat]=meshgrid(xvec,yvec); %the coord matrices
    objradius=sqrt(xmat.^2+ymat.^2);

    %plane Hol
    hxvec=-N/2*a_hol:a_hol:(N/2-1)*a_hol; %element N/2+1 has coord 0
    hyvec=hxvec;
    [hxmat,hymat]=meshgrid(hxvec,hyvec); %the coord matrices
    holradius=sqrt(hxmat.^2+hymat.^2);

    %Plane Far
    a_far=lambda_sample*L1/(N*a_obj); %sample interval in plane Far
    fxvec=-N/2*a_far:a_far:(N/2-1)*a_far; %element N/2+1 has coord 0
    fyvec=fxvec;
    [fxmat,fymat]=meshgrid(fxvec,fyvec); %the coord matrices
    farradius=sqrt(fxmat.^2+fymat.^2);
```

57

```matlab
%Plane of Reference
a_ref=a_far*L1/Lref;
refxvec=-N/2*a_ref:a_ref:(N/2-1)*a_ref; %element N/2+1 has coord 0
refyvec=refxvec;
[refxmat,refymat]=meshgrid(refxvec,refyvec); %the coord matrices
refradius=sqrt(refxmat.^2+refymat.^2);

%The object revisited
F=L1/L2.*exp(i*k*(L2-L1)).*exp(i*k/2*farradius.^2*(1/L2-1/L1));
Hol_plane=sqrt(I_hol).*exp(i*k*holradius.^2/(2*L2));
E_obj_revisited=exp(-i*k.*objradius.^2/(2*L1))
.*ifft2c(F.*fft2c(Hol_plane));

I_obj_rev=abs(E_obj_revisited)

title(['Distance between Object and Hologram:
    ',num2str((min_L-step)/10^4),'cm'])
figure(j)
colormap(gray)

image(xvec,yvec,I_obj_rev.*4)
min_L=min_L+step;
j=j+1;
end
```

Appendix C

The STAR 1 CCD System

This is merely a short supplement aimed at aiding anyone attempting to take and process pictures with the STAR 1 CCD. Setting up the system and running it independant of a computer should not cause any troubles since the steps are well covered in the manual. The problems are, however, bound to come about when the goal is to take pictures with the aid of a computer.

The STAR is connected to a computer via GPIB and the software that was necessary to run the STAR from a computer was found on the computer atom-laser 3. These programs are Zstar for taking the pictures, Star2bmp for converting the pictures into a useful format, and GPIB Spy which monitors the information tranfer between the CCD and the computer.

How to do:

Start Zstar. Pictures are taken with the expose icon and saved under the save icon. For some reason it is not possible to save the images with a suffix.

Start Star2bmp. Click on File/Open images. To get to the pictures the file settings must be changed to All Files (*.*). Now just save the pictures with the suffix bmp.

This maybe won't work. For some strange reason starting GPIB Spy helps. If for some reason the program isn't installed, I installed it through running

Triggering the STAR CCD

It was found that a slightly modified inverted pulse works best when triggering the CCD. It must be at least 0.9 V high and 20 microseconds long. Further it has to be made sure that no new signal comes in during the time the system is eptying the CCD chip. That takes approximately 2,5 s. Also it has been found that a trigger pulse affects the system even though the Trig function isn't activated.